2. Methods

2.1. Participants

We studied three probands from three unrelated families with MMD, a carrier of RNF213 R4810K and seven controls. Details of the patients were described previously [8] and in Table S1. We obtained written informed consent from all participants in this study. Our study was approved by the Institutional Ethical Review Board of Kyoto University.

2.2. Cell culture and transfection

Fibroblasts and HeLa cells were maintained in Dulbecco's Minimal Essential Medium (DMEM; Invitrogen, Tokyo, Japan) containing 10% fetal bovine serum (FBS; Japan Bioserum, Hiroshima, Japan). Fibroblasts from passages 3–5 were used for all experiments. Induced pluripotent stem cells (iPSCs) were maintained as previously reported [8,9].

An mCherry-tagged wild-type RNF213 or an mCherry-tagged RNF213 R4810 K was cloned into pcDNA3.1 (Invitrogen) (Fig. S1) [8]. To monitor the localization of MAD2, HeLa cells stably expressing EGFP-MAD2 were used. MAD2 cDNA cloned into pEGFP-C1 (Clontech Laboratories, Palo Alto, CA, USA) was introduced into HeLa cells, and a G418-resistant clone was verified by western blotting and fluorescent microscopy. The plasmid was introduced into HeLa cells using Lipofectamine 2000 (Invitrogen) and successfully transfected cells selected with 500 μg/ml G418 (Nacalai Tesque, Kyoto, Japan) for 10 days.

Transfection of small interfering RNAs (siRNAs) was conducted using Dharmafect (#1 or #3; Dharmacon, Lafayette, CO, USA) as previously reported [8]. We purchased and used RNF213 siRNA (Santa Cruz Biotechnology) and MAD2 siRNA (Santa Cruz Biotechnology) with control siRNA-A (Santa Cruz Biotechnology) used as controls.

2.3. Karyotyping

For karyotyping, fibroblasts from six controls (Control 1 to Control 6), one carrier, and three patients were treated with nocodazole (100 ng/ml) for 72 h. Well-isolated chromosomes were chosen and counted three times for each chromosome set. For each fibroblast culture, duplicate karyotyping experiments were conducted. For MAD2 staining, fibroblasts were treated with nocodazole (100 ng/ml) for 72 h, fixed with 4% paraformaldehyde and permeabilized in phosphate-buffered saline (PBS) containing 0.2% Triton X-100. An anti-MAD2 antibody (Covance, Berkeley, CA, USA) was used for immunostaining.

To evaluate chromosomal instability, six iPSC clones from controls (Control 1 to Control 7 except Control 4) and four from a carrier and patients were karyotyped (Table S1).

2.4. Colony formation assays

Following transfection, HeLa cells were reseeded at densities of 1×10^3 to 2.7×10^4 cells/100-mm dish and maintained in DMEM with 10% FBS for 5 days. Medium containing G418 (Nacalai Tesque) was exchanged twice a week. After 10 days, resistant colonies were scored using formalin fixation and crystal violet staining.

2.5. Time-lapse imaging using confocal laser scanning microscopy

Transfected HeLa cells and iPSECs were plated on 35-mm glass-bottom culture dishes. Time-lapse 3D imaging was performed using an FV10i confocal microscope (Olympus, Tokyo, Japan) at 37 °C/5% CO_2. The recording interval was 40 min, and Z-stack images were generated with Fluoview (Olympus).

2.6. Western blotting

Samples were subjected to immunoblotting using the anti-RNF213 antibody, which we generated previously [8], anti-MAD2, anti-dsRed (BD Biosciences), or anti-β-actin (Abcam, Cambridge, UK) antibodies. Quantitation was conducted using Image J software.

2.7. Co-immunoprecipitation of MAD2 with RNF213

HeLa cells transiently expressing the wild-type RNF213 mCherry or RNF213 R4810K mCherry or naïve HeLa cells were lysed in RIPA buffer without sodium dodecyl sulfate (SDS) but with protease inhibitors (Nacalai Tesque). Cell lysates from 4×10^6 cells were incubated with protein A agarose (Santa Cruz Biotechnology) for 30 min at 4 °C with normal mouse immunoglobulin G (IgG; MBL, Nagoya, Japan). After magnetic separation, beads were discarded and supernatants incubated for 4 h at 4 °C with a monoclonal anti-dsRed or polyclonal anti-RNF213 antibody [8] followed by magnetic beads for 4 h. Beads were washed three times with lysis buffer, and bound proteins dissolved in SDS sample buffer at 95 °C for 5 min, subjected to SDS polyacrylamide gel electrophoresis (PAGE) and analyzed by western blotting with anti-MAD2 antibody.

2.8. Statistical analysis

Results are presented as the mean ± standard deviation (SD) unless otherwise stated. Differences between groups were analyzed using analysis of variance (ANOVA), followed by Tukey's honestly significant difference test for comparisons involving more than two means (SAS Institute Inc., Cary, NC, USA). The variance in chromosome numbers as determined by karyotyping was compared with controls using an F-test. Subcellular localization of MAD2 was categorized into four groups and compared with controls using Fisher's exact test with Bonferroni correction. A p-value with Bonferroni correction less than 0.05 was considered statistically significant.

3. Results

3.1. Effects of RNF213 R4810K overexpression

mCherry-tagged wild-type RNF213 and/or RNF213 R4810K proteins (Fig. S1) were overexpressed in HeLa cells (Fig. S2A and B). Localization of exogenous RNF213 R4810K was similar to that of exogenous and endogenous wild-type RNF213, where proteins were observed in the cytoplasm around the nucleus (Fig. S2B). Overexpression of RNF213 R4810K highly repressed colony formation units of HeLa cells (Fig. S2C). In contrast, RNAi-mediated depletion of RNF213 in HeLa cells did not repress colony formation units (Fig. S2D).

To understand better the causes underlying inhibition of cell proliferation, cell cycle distribution of HeLa cells expressing wild-type RNF213 and RNF213 R4810K were monitored. Overexpression of RNF213 R4810K caused a G2/M-plus-higher-DNA-content (4N>) accumulation in HeLa cells (Fig. S3), but overexpression of wild-type of RNF213 did not. Live imaging analyses showed that mitotic stages were severely delayed in HeLa cells overexpressing RNF213 R4810K (Fig. 1A–C). In cells overexpressing the control vector, wild-type RNF213, control siRNA or RNF213 siRNA, the mean time from prometaphase to metaphase was 37 ± 10 min: The mean time

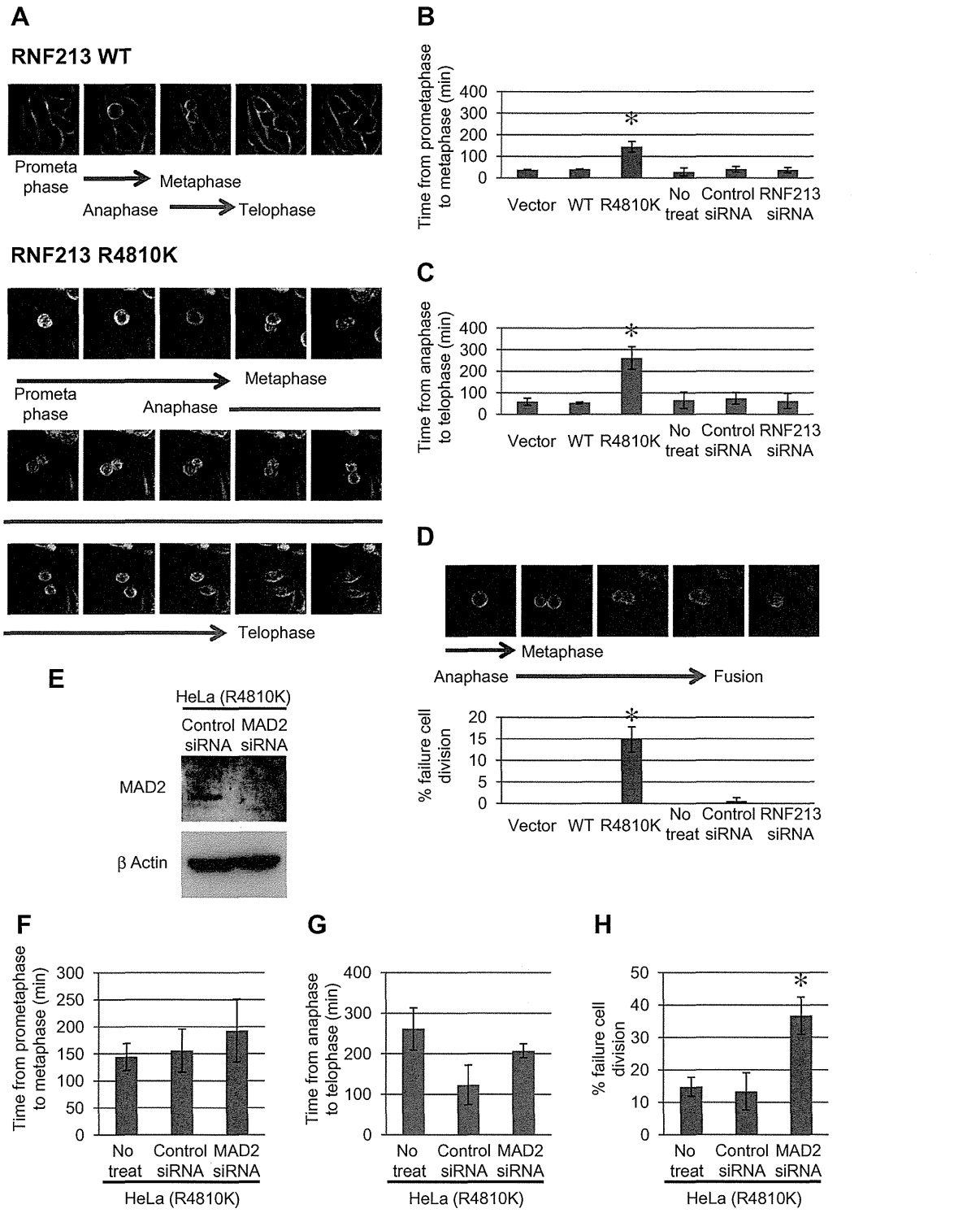

Fig. 1. Time-lapse imaging of HeLa cells transfected with wild-type RNF213 and RNF213 R4810K, or control siRNA, RNF213 siRNA and MAD2 siRNA. (A) Representative time-lapse images showing wild-type RNF213 and RNF213 R4810K. Images were obtained every 40 min. (E) Western blot analysis of HeLa cells overexpressing RNF213 R4810K with MAD2 siRNA transfection. (B, C, F, G) The period of time from prometaphase to metaphase, and from anaphase to telophase. A total of 20 cells were observed in three areas for each group. (D, H) Failed cell division in HeLa cells overexpressing RNF213 R4810K transfected with control siRNA and MAD2 siRNA. Cells ($n = 40$) were counted in three areas for each group. Values are presented as means ± SDs. $^*p < 0.05$.

from anaphase to telophase was 63 ± 24 min (Fig. 1B and C). In contrast, for cells overexpressing RNF213 R4810K, progression from prometaphase to metaphase was 144 ± 25 min, while the progression from anaphase to telophase was 261 ± 52 min (Fig. 1B and C). Overexpression of RNF213 R4810K resulted in several daughter cells that failed to complete cell division. For 14.8 ± 2.9% of the total cell population, cytokinesis failed to occur (Fig. 1D).

We investigated whether activation of spindle checkpoint was responsible for the delayed mitotic progression phenotype in HeLa cells overexpressing RNF213 R4810K. We inhibited spindle checkpoint by depletion of MAD2, which senses mitotic progression, and

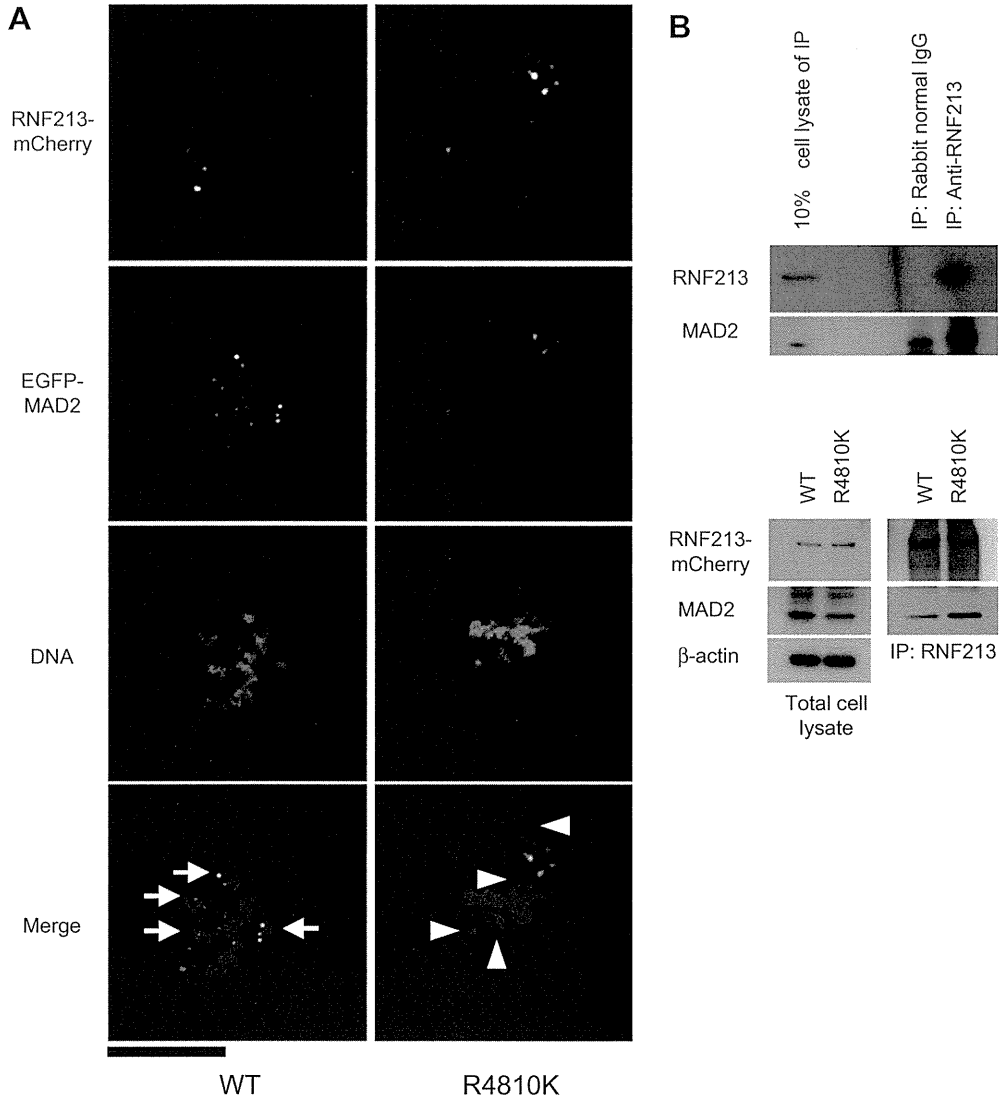

Fig. 2. Colocalization of RNF213 R4810K with MAD2 at prometaphase. (A) MAD2 localization in HeLa cells overexpressing wild-type RNF213 and RNF213 R4810K. Wild-type RNF213-mCherry (left panels; WT) or RNF213 R4810K-mCherry (right panels; R4810K) plasmids were introduced into HeLa cells stably expressing EGFP-MAD2. Red, green and blue staining corresponded to signals for RNF213-mCherry, EGFP-MAD2 and DNA, respectively. MAD2-positive lagging chromosomes in cells overexpressing wild-type RNF213 are indicated by arrows. Lagging chromosomes without MAD2 signals in cells overexpressing RNF213 R4810K are indicated by arrowheads. The scale bar indicates 20 μm. (B) Upper panel: HeLa cells were lysed and subjected to immunoprecipitation (IP) using rabbit normal IgG or an anti-RNF213 antibody. Ten-fold diluted cell lysate and the immunoprecipitated samples were immunoblotted using anti-RNF213 and anti-MAD2 antibodies. Lower panel: HeLa cells transiently expressing wild-type RNF213-mCherry (WT) or RNF213 R4810K-mCherry (R4810K) were lysed and subjected to IP using an anti-dsRed antibody. Total cell lysate and the IP samples were immunoblotted using anti-dsRed and anti-MAD2 antibodies. β-Actin was used as a loading control. (For interpretation of the references to color in this figure legend, the reader is referred to the web version of this article.)

conducted live image analysis (Fig. 1E–G). Depletion of MAD2 did not shorten the time in mitosis. In contrast, the mitotic failure rate was further increased by depletion of MAD2 in HeLa cells overexpressing RNF213 R4810K (Fig. 1H).

The localization of RNF213 was also analyzed during the mitotic phase by tracking MAD2 localization. In cells transfected with wild-type RNF213, MAD2 was localized onto the kinetochore during prometaphase, and translocated to centrosomes with RNF213 during the metaphase to anaphase transition (Figs. 2A and S4) as reported [10,11]. Signals corresponding to mCherry-tagged wild-type RNF213 were colocalized with MAD2 on mitotic microtubules around centrosomes during metaphase (Fig. S4). In contrast, we observed abnormal localization of MAD2 in cells overexpressing RNF213 R4810K. During prometaphase, MAD2 signals were not observed onto kinetochores but colocalized with RNF213 R4810K on mitotic microtubules around centrosomes (Fig. 2A). Localization of signals corresponding to mCherry-tagged RNF213 R4810K was, however, similar to that in cells overexpressing wild-type RNF213 during metaphase (Fig. S4).

The colocalization of MAD2 and RNF213 R4810K led us to investigate whether RNF213 R4810K or wild-type RNF213 could form a complex with MAD2. Both endogenous and exogenous wild-type RNF213 were co-immunoprecipitated by an anti-RNF213 antibody with endogenous MAD2 from HeLa cell extracts (Fig. 2B). A greater quantity of MAD2 was co-immunoprecipitated with the complex containing RNF213 R4810K compared with that containing wild-type RNF213. These data collectively suggest that the effects of MAD2 depletion on mitotic failure phenotype can override the mislocalization of MAD2 induced by overexpression of RNF213 R4810K in an additive manner while the effect on delayed mitotic progression phenotype is saturated.

3.2. iPSC karyotypes and mitotic abnormality in human fibroblasts

iPSCs from six fibroblast clones had normal karyotypes, but those from three MMD patients had abnormal karyotypes (Table S1, Fig. S5). The incidence of abnormal karyotypes in iPSC clones from subjects with RNF213 R4810K was 75% (3/4), while none of the six iPSC clones with wild-type RNF213 (0/6) had abnormal karyotypes (Fisher's exact test, $p < 0.03$). We then examined mitotic defects in primary fibroblasts from controls, the unaffected carrier and MMD patients (Table S1). All fibroblasts had normal karyotypes. We also searched for potential mitotic defects that may have been inherent in primary fibroblasts in patients with MMD by activating the spindle checkpoint with nocodazole. MAD2 signals and mitotic morphology were observed 72 h after treatment with nocodazole. Treatment with nocodazole depolymerizes microtubules and attached microtubules are detracted from kinetochores. Therefore, MAD2 should have been mobilized onto unattached kinetochores. In fact, in control cells, the majority of MAD2 was observed at the kinetochores. However, large quantities of MAD2 did not bind to the kinetochores of lagging chromosomes (Fig. 3) in fibroblasts from patients with RNF213 R4810K ($n = 3$, $61.0 \pm 8.2\%$) compared with those from controls ($n = 6$, $13.1 \pm 7.7\%$; $p < 0.01$). Furthermore, aneuploidy was observed more frequently in fibroblasts from MMD patients than in controls (Fig. 4A). Even under the condition of activated spindle checkpoint by nocodazole, distances of sister chromatids were widened in patient 1 and patient 2 and sister chromatids were separated completely in patient 3 (Fig. 4B). Premature sister chromatid separation can induce karyotype abnormality. Taken together these observations, the mislocalization of MAD2, aneuploidy and premature sister chromatid separation, consistently suggest mitotic abnormalities.

Next live image analyses for iPSECs from patients, Patient 1(GA), 2 (AA) and 3 (AA), an unaffected carrier (GA) and controls, Control 1 and 2 (GG) were conducted (Fig. 4C). The mean time (min) from prometaphase to metaphase was significantly longer (GA; 79.2 ± 72.1 or AA; 94.4 ± 86.3) for iPSECs from patients and unaffected carrier than from controls (42.0 ± 30.3; $p < 0.05$). However, the mean time from metaphase to anaphase for iPSECs from patients and unaffected carrier was not different from that for iPSECs from controls ($p > 0.05$). It is interesting that the mitotic failure rate (%) was also significantly higher for iPSECs from the patients and unaffected carrier (GA; 13.0 ± 3.2 or AA; 21.2 ± 4.0) than from the controls (1.9 ± 3.2; $p < 0.05$). The phenomena observed in HeLa cells overexpressing RNF213 R4810K were recaptured in iPSECs heterozygous and homozygous for RNF213 R4810K, suggesting that mitotic abnormality is genuinely associated with RNF213 R4810K.

4. Discussion

In this study, we demonstrated that RNF213 R4810K adversely affected the localization of MAD2 to the kinetochore during mitosis. Furthermore, RNF213 colocalized with MAD2 by confocal microscopy and immunoprecipitation confirmed both endogenous and exogenous wild-type RNF213 and RNF213 R4810K formed complexes with MAD2. The MAD2 complex with RNF213 R4810K captured a greater quantity of MAD2 than the complex with wild-type RNF213, suggesting a larger capturing capacity. The abnormal localization of MAD2 and mitotic abnormality were confirmed in primary fibroblasts from MMD patients. Furthermore, we observed more frequent karyotype abnormality in iPSCs from MMD patients compared with wild-type controls.

These findings indicate that RNF213 R4810K induces phenotypes associated with mitotic abnormalities. It is well known that genetic defects in cell cycle-related proteins are associated with steno-occlusive lesions around the Circle of Willis. These include Ras-MAPK pathway-related diseases (neurofibromatosis 1, Noonan syndrome, Castelo syndrome, Cranio-facio-cutaneous syndrome, and Alagille syndrome [12–14]) and cell cycle-related diseases (microcephalic osteodysplastic primordial dwarfism type II, Seckel syndrome and X-related moyamoya syndrome) [15]. The majority of cell cycle-related diseases are often accompanied by somatic undergrowth. It is likely that cell cycle defects elevate the risk of cell death or mitotic failure due to defective mitosis and chromosomal missegregation, which may be a common inherent risk factor among diseases associated with moyamoya syndrome and MMD. This would adversely affect multiple organs, including the vascular system. In contrast, MMD is not complicated by somatic undergrowth. We speculate that mitotic defects in RNF213 R4810K carriers specifically emerge in vascular endothelial cells.

The current study demonstrated an elevated mitotic failure rate in iPSECs from MMD patients. When ECs are damaged, they may be peeled off from the vascular bed and then denudated vascular areas emerge. Such vascular denudation should be recovered by migration and proliferation of circulating endothelial progenitor cells. Unless otherwise, migration and proliferation of vascular smooth muscle cells (VSMCs) occur subsequently, resulting in intimal hyperplasia. It may be considered a limitation of our work that we did not investigate VSMCs. However, given the pathological model of the vascular injury induced by radiation [16], which is known to cause steno-occlusive lesion in intracranial artery [3], an initial pathological process in MMD may be reasonably assumed to be mediated by mitotic failure of endothelial cells (ECs) followed by the excessive proliferation of VSMCs. The interactions between ECs and VSMCs play key roles in maintaining vascular structure and the function of vessels [16]. VSMC migration, proliferation, and differentiation are critical processes involved in intimal hyperplasia and are regulated by ECs [16]. Thus, mitotic failure may impair the crosstalk between ECs and VSMCs in patients with MMD. Further studies focusing on cell cycle defects in VSMCs and the crosstalk between VSMCs and endothelial cells are necessary.

In the current study, delayed mitotic progression phenotypes of HeLa cells overexpressing RNF213 R4810K or of iPSECs from patients was consistently observed. To investigate whether spindle checkpoint activation is responsible for the delayed mitotic progression phenotype, the MAD2 signaling pathway was inhibited. Depletion of MAD2 did not shorten time in mitosis or induce mitotic exit in cells overexpressing RNF213 R4810K, indicating that spindle checkpoint may be inactivated in those cells. Depletion of MAD2, however, could override the mitotic failure phenotype of HeLa cells overexpressing RNF213 R4810K in an additive manner. These observations suggest overexpression of RNF213 R4810K causes MAD2 mislocalization and leads to inactivation of MAD2 function, which is further impaired by depletion of MAD2 in the phenotype of the mitotic failure. Previously, we reported that RNF213 R4810K suppressed gene expression of *Securin*, *SKA3*, *SGO1*, *CDC20* and *BUB1*[8]. It should be noted that depletion of *SKA3* and *SGO1* cause mitotic delays and premature sister chromatid separation [17]. Taken together, for mechanisms of mitotic abnormalities, a simple and straightforward explanation would be to assume that because *Securin* has dual mechanisms of separase regulation [18] and depletion of *Securin* slowed mitotic progression [19], RNF213 R4810K slowed mitotic progression by down-regulation of *Securin* and caused mitotic abnormalities by MAD2 mislocalization [20]. However, we cannot ignore other possibilities because other down regulated genes may cause mitotic abnormalities in a synergistic manner or an antagonistic manner. The most substantial event in mitotic abnormalities, however, is likely associated with the down regulation of a group of mitosis

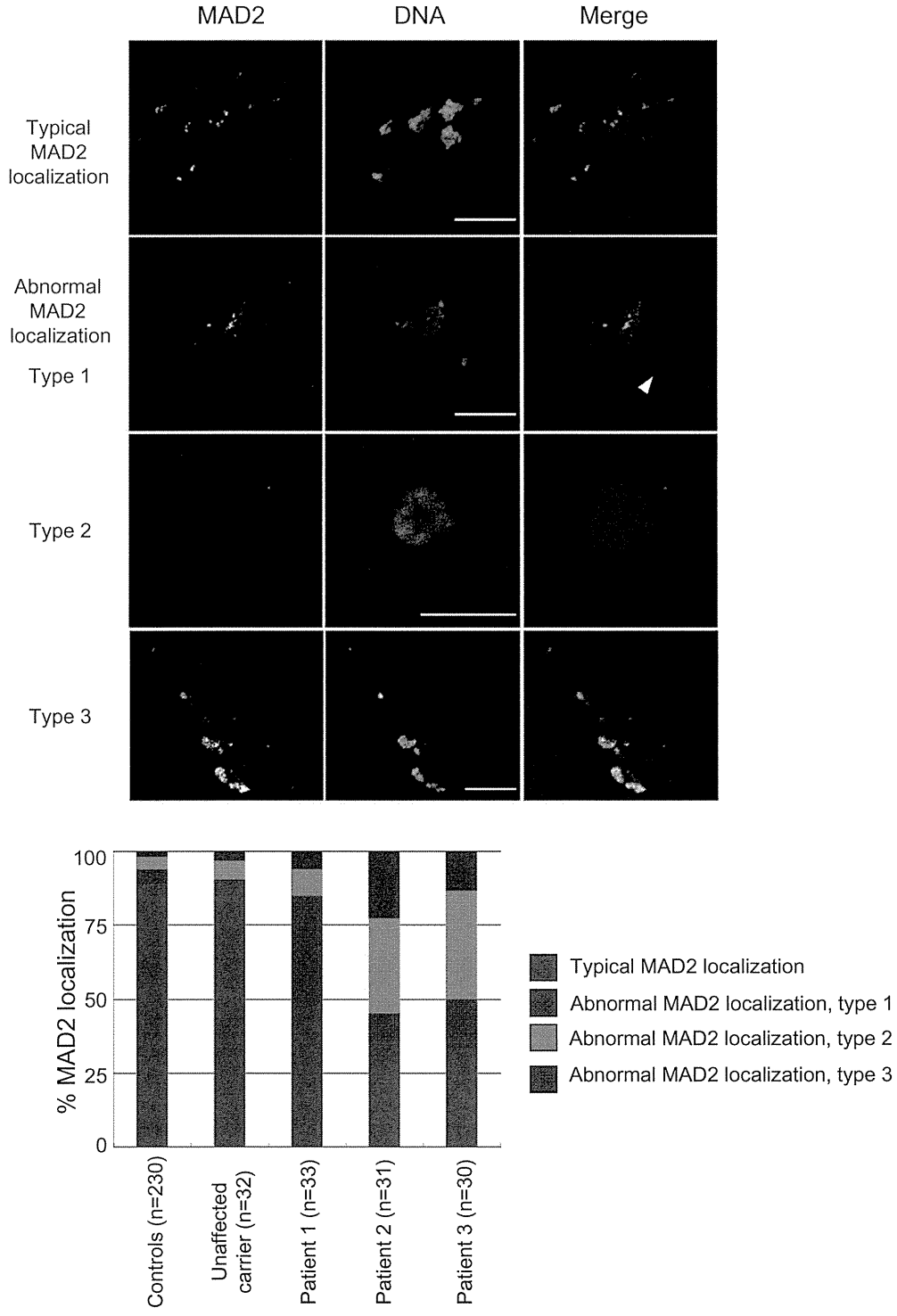

Fig. 3. Subcellular localization of MAD2 in fibroblasts from MMD patients at prometaphase. Fibroblasts from MMD patients ($n = 3$), an unaffected carrier ($n = 1$), or controls ($n = 6$) treated with nocodazole for 72 h were incubated with an antibody against MAD2. The numbers of examined chromosomes are shown in parentheses. For each subject, more than 30 chromosomes were investigated. Typical MAD2 signals (green) and nuclei (blue) in MMD fibroblasts are shown in the top panels. The scale bar represents 10 μm. Abnormal MAD2 staining patterns are shown in the lower panel. Abnormal MAD2 localization type 1 refers to MAD2-positive cells with MAD2-negative lagging chromosomes (arrowhead). Abnormal MAD2 localization type 2 refers to MAD2-negative cells. Abnormal MAD2 localization type 3 was defined as a distribution pattern of MAD2 that was not spotty, yet the protein was present and spread across the entire chromosome. The frequencies of the different MAD2 staining patterns in MMD fibroblasts were compared with controls using Fisher's exact test followed by Bonferroni correction. $p = 1.00$, unaffected carrier vs. controls; $p = 3.19 \times 10^{-11}$, patient 1 vs controls; $p = 8.77 \times 10^{-7}$, patient 2 vs controls; $p = 5.54 \times 10^{-10}$, patient 3 vs controls. (For interpretation of the references to color in this figure legend, the reader is referred to the web version of this article.)

associated genes by RNF213 R4810K. Further studies are needed to understand the mechanisms of RNF213 R4810K-induced down regulation of mitosis-associated genes and subsequent signaling deviations that induce mitotic abnormalities.

We observed an inhibition of cellular proliferation *in vitro*, but not in *ex vivo* studies [8]. We attributed these differences to acute and chronic effects. Acutely, there is very little adaptation to RNF213 R4810K overexpression; however, in chronic cases the cells

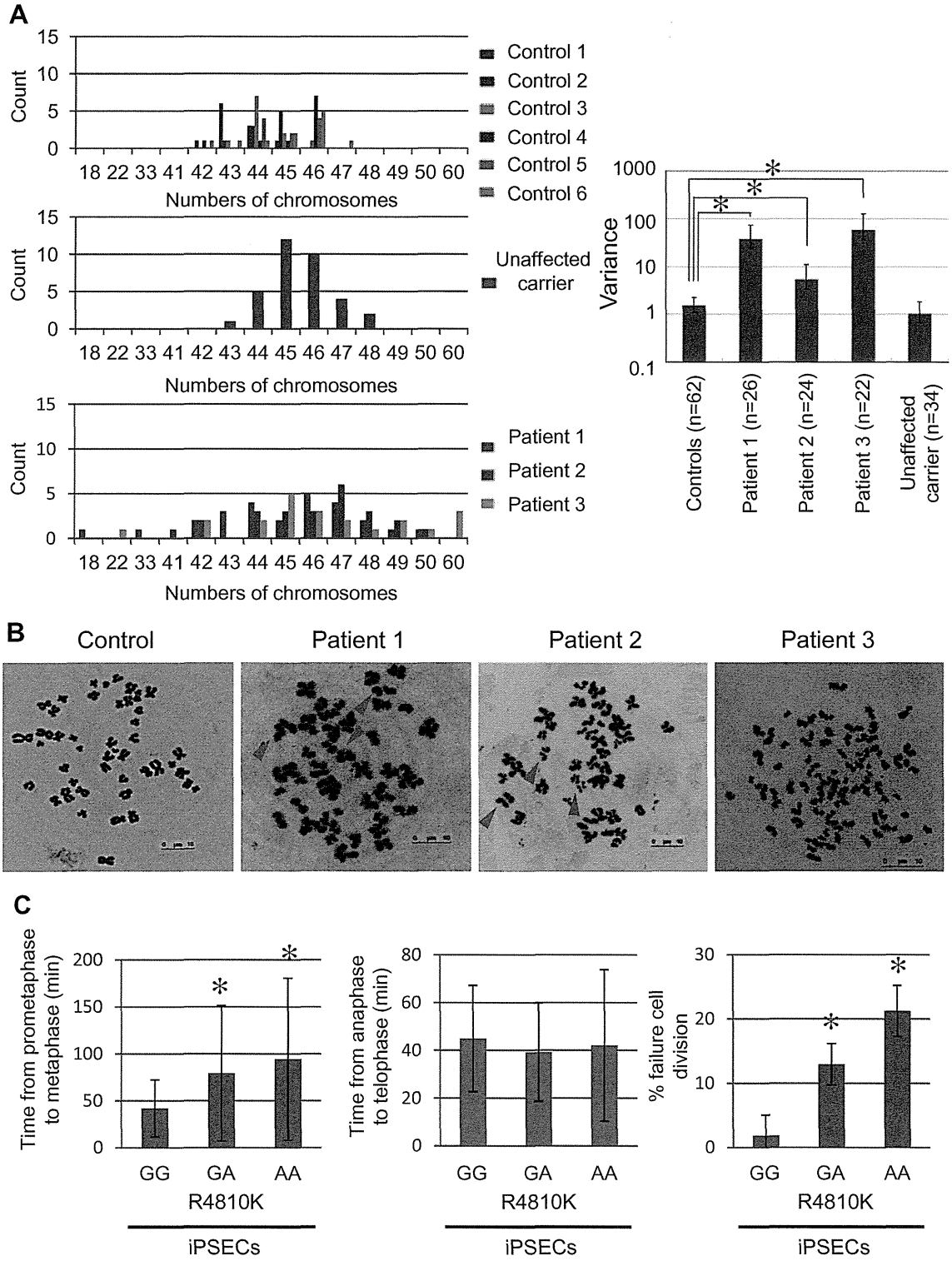

Fig. 4. Mitotic abnormality in fibroblasts and time-lapse imaging of iPSECs from MMD patients. (A) Karyotypes of MMD fibroblasts. Fibroblasts from MMD patients, the unaffected carrier or controls treated with nocodazole for 72 h were subjected to Giemsa staining. Fibroblasts from the controls (upper), carriers (middle), and MMD patients (lower) can be clearly seen. The variance in chromosome number is presented with a 95% confidence interval (right panel). Heterogeneity in the variance was tested using the *F*-test with Bonferroni correction for equality of variance. $^*p < 0.001$ using the *F*-test. (B) Typical morphologies of chromosomes stained with Giemsa in fibroblasts from MMD patients and controls. Prematurely separated chromosomes in the fibroblasts from patients 1 and 2 are indicated by arrowheads. Completely separated chromosomes in the fibroblasts from patient 3 are shown in the right panel. The typical morphology of fibroblasts from controls is presented in the left panel. The scale bar indicates 10 μm. (C) Time-lapse imaging of iPSECs from MMD patients and an unaffected carrier (GA or AA genotype) and controls (GG genotype). The period of time from prometaphase to metaphase, and from anaphase to telophase, and failed cell division were evaluated. Values are presented as means ± SDs. $^*p < 0.05$.

may adapt for the gain of function effects of this protein and mask the proliferative defects. Such discrepancies are often observed between acute and chronic effects [21–23].

In conclusion, this study demonstrated the sequestration of MAD2 by RNF213 R4810K during mitosis. The resultant defects including mitotic abnormalities were considered to increase genomic instability and thus be risk factors for MMD.

Funding sources

This work was supported by grants from the Ministry of Education, Culture, Sports, Science and Technology of Japan (Nos. 17109007 and 22249020 to Dr. Koizumi). This research was partially supported by the Japan Society for the Promotion of Science through its Funding Program for World-Leading Innovative R&D on Science and Technology (FIRST Program to Dr. Osafune).

Acknowledgments

We are grateful to Drs. Wanyang Liu, Shanika Nanayakkara, STMLD Senevirathna (Kyoto University Graduate School of Medicine) and Sasatani (Toyoshima) M (Hiroshima University) for their discussion.

Appendix A. Supplementary data

Supplementary data associated with this article can be found, in the online version, at http://dx.doi.org/10.1016/j.bbrc.2013.08.067.

References

[1] J. Suzuki, A. Takaku, Cerebrovascular "moyamoya" disease. Disease showing abnormal net-like vessels in base of brain, Arch. Neurol. 20 (1969) 288–299.
[2] K. Takeuchi, K. Shimizu, Hypogenesis of bilateral internal carotid arteries, Brain Nerv. 9 (1957) 37–43.
[3] S. Kuroda, K. Houkin, Moyamoya disease: current concepts and future perspectives, Lancet Neurol. 7 (2008) 1056–1066.
[4] W. Miao, P.L. Zhao, Y.S. Zhang, H.Y. Liu, Y. Chang, J. Ma, Q.J. Huang, Z.X. Lou, Epidemiological and clinical features of Moyamoya disease in Nanjing, China, Clin. Neurol. Neurosurg. 112 (2010) 199–203.
[5] R.M. Scott, E.R. Smith, Moyamoya disease and moyamoya syndrome, N. Engl. J. Med. 360 (2009) 1226–1237.
[6] A. Veeravagu, R. Guzman, C.G. Patil, L.C. Hou, M. Lee, G.K. Steinberg, Moyamoya disease in pediatric patients: outcomes of neurosurgical interventions, Neurosurg. Focus 24 (2008) E16.
[7] W. Liu, D. Morito, S. Takashima, Y. Mineharu, H. Kobayashi, T. Hitomi, H. Hashikata, N. Matsuura, S. Yamazaki, A. Toyoda, K. Kikuta, Y. Takagi, K.H. Harada, A. Fujiyama, R. Herzig, B. Krischek, L. Zou, J.E. Kim, M. Kitakaze, S. Miyamoto, K. Nagata, N. Hashimoto, A. Koizumi, Identification of RNF213 as a susceptibility gene for moyamoya disease and its possible role in vascular development, PLoS ONE 6 (2011) e22542.
[8] T. Hitomi, Habu, T., Kobayashi, H., Okuda, H., Harada, HK, Osafune, K., Taura, D., Sone, M., Adaka, I., Ameku, T., Watanabe, A., Kasahara, T., Sudo, T., Shiota, F., Hashikata, H., Takagi, Y., Morito, D., Miyamoto, S., Nakao K., and Koizumi, A., Down-regulation of Securin by the variant RNF213 R4810K may likely reduce angiogenic activity of induced pluripotent stem cells- derived vascular endothelial cells from moyamoya patients, Biochem. Biophys. Res. Commun. **438**, (2013), 13-19.
[9] K. Takahashi, K. Tanabe, M. Ohnuki, M. Narita, T. Ichisaka, K. Tomoda, S. Yamanaka, Induction of pluripotent stem cells from adult human fibroblasts by defined factors, Cell 131 (2007) 861–872.
[10] B.J. Howell, D.B. Hoffman, G. Fang, A.W. Murray, E.D. Salmon, Visualization of Mad2 dynamics at kinetochores, along spindle fibers, and at spindle poles in living cells, J. Cell Biol. 150 (2000) 1233–1250.
[11] Y. Li, R. Benezra, Identification of a human mitotic checkpoint gene: hsMAD2, Science 274 (1996) 246–248.
[12] W.E. Tidyman, K.A. Rauen, Noonan, Costello and cardio-facio-cutaneous syndromes: dysregulation of the Ras-MAPK pathway, Exp. Rev. Mol. Med. 10 (2008) e37.
[13] B.M. Kamath, N.B. Spinner, K.M. Emerick, A.E. Chudley, C. Booth, D.A. Piccoli, I.D. Krantz, Vascular anomalies in Alagille syndrome: a significant cause of morbidity and mortality, Circulation 109 (2004) 1354–1358.
[14] M. Noseda, L. Chang, G. McLean, J.E. Grim, B.E. Clurman, L.L. Smith, A. Karsan, Notch activation induces endothelial cell cycle arrest and participates in contact inhibition: role of p21Cip1 repression, Mol. Cell. Biol. 24 (2004) 8813–8822.
[15] A. Koizumi, H. Kobayashi, T. Hitomi, Genes associated with moyamoya syndrome and disease, No Shinkei Geka 40 (2012) 105–118.
[16] F. Milliat, A. Francois, M. Isoir, E. Deutsch, R. Tamarat, G. Tarlet, A. Atfi, P. Validire, J. Bourhis, J.C. Sabourin, M. Benderitter, Influence of endothelial cells on vascular smooth muscle cells phenotype after irradiation: implication in radiation-induced vascular damages, Am. J. Pathol. 169 (2006) 1484–1495.
[17] J.R. Daum, J.D. Wren, J.J. Daniel, S. Sivakumar, J.N. McAvoy, T.A. Potapova, G.J. Gorbsky, Ska3 is required for spindle checkpoint silencing and the maintenance of chromosome cohesion in mitosis, Curr. Biol. 19 (2009) 1467–1472.
[18] N.C. Hornig, P.P. Knowles, N.Q. McDonald, F. Uhlmann, The dual mechanism of separase regulation by securin, Curr. Biol. 12 (2002) 973–982.
[19] L.J. Holt, A.N. Krutchinsky, D.O. Morgan, Positive feedback sharpens the anaphase switch, Nature 454 (2008) 353–357.
[20] L. Michel, E. Diaz-Rodriguez, G. Narayan, E. Hernando, V.V. Murty, R. Benezra, Complete loss of the tumor suppressor MAD2 causes premature cyclin B degradation and mitotic failure in human somatic cells, Proc. Natl. Acad. Sci. USA 101 (2004) 4459–4464.
[21] F. Iovino, L. Lentini, A. Amato, A. Di Leonardo, RB acute loss induces centrosome amplification and aneuploidy in murine primary fibroblasts, Mol. Cancer 5 (2006) 38.
[22] J. Mei, X. Huang, P. Zhang, Securin is not required for cellular viability, but is required for normal growth of mouse embryonic fibroblasts, Curr. Biol. 11 (2001) 1197–1201.
[23] K. Pfleghaar, S. Heubes, J. Cox, O. Stemmann, M.R. Speicher, Securin is not required for chromosomal stability in human cells, PLoS Biol. 3 (2005) e416.

Biochemical and Biophysical Research Communications 438 (2013) 13–19

Contents lists available at SciVerse ScienceDirect

Biochemical and Biophysical Research Communications

journal homepage: www.elsevier.com/locate/ybbrc

Downregulation of Securin by the variant RNF213 R4810K (rs112735431, G>A) reduces angiogenic activity of induced pluripotent stem cell-derived vascular endothelial cells from moyamoya patients

Toshiaki Hitomi [a,1], Toshiyuki Habu [b,1], Hatasu Kobayashi [a], Hiroko Okuda [a], Kouji H. Harada [a], Kenji Osafune [c], Daisuke Taura [d], Masakatsu Sone [d], Isao Asaka [c], Tomonaga Ameku [c], Akira Watanabe [c], Tomoko Kasahara [c], Tomomi Sudo [c], Fumihiko Shiota [c], Hirokuni Hashikata [e], Yasushi Takagi [e], Daisuke Morito [f], Susumu Miyamoto [e], Kazuwa Nakao [d], Akio Koizumi [a,*]

[a] Department of Health and Environmental Sciences, Kyoto University, Kyoto, Japan
[b] Radiation Biology Center, Kyoto University, Kyoto, Japan
[c] Center for iPS Cell Research and Application (CiRA), Kyoto University, Kyoto, Japan
[d] Department of Medicine and Clinical Science, Kyoto University, Kyoto, Japan
[e] Department of Neurosurgery, Kyoto University,Kyoto, Japan
[f] Faculty of Life Sciences, Kyoto Sangyo University, Kyoto, Japan

ARTICLE INFO

Article history:
Received 30 June 2013
Available online 12 July 2013

Keywords:
Moyamoya disease
iPS cells
Endothelium
Angiogenesis
RNF213
Securin

ABSTRACT

Moyamoya disease (MMD) is a cerebrovascular disease characterized by occlusive lesions in the circle of Willis. The RNF213 R4810K polymorphism increases susceptibility to MMD. Induced pluripotent stem cells (iPSCs) were established from unaffected fibroblast donors with wild-type RNF213 alleles, and from carriers/patients with one or two RNF213 R4810K alleles. Angiogenic activities of iPSC-derived vascular endothelial cells (iPSECs) from patients and carriers were lower (49.0 ± 19.4%) than from wild-type subjects ($p < 0.01$). Gene expression profiles in iPSECs showed that Securin was down-regulated ($p < 0.01$) in carriers and patients. Overexpression of RNF213 R4810K downregulated Securin, inhibited angiogenic activity (36.0 ± 16.9%) and proliferation of humanumbilical vein endothelial cells (HUVECs) while overexpression of RNF213 wild type did not. Securin expression was downregulated using RNA interference techniques, which reduced the level of tube formation in iPSECs and HUVECs without inhibition of proliferation. RNF213 R4810K reduced angiogenic activities of iPSECs from patients with MMD, suggesting that it is a promising *in vitro* model for MMD.

1. Introduction

Moyamoya disease (MMD) is an idiopathic cerebrovascular disease. It is characterized by occlusive lesions at the terminal portion of internal carotid arteries in the circle of Willis, with compensatory development of a fine vascular network that resembles "puffs of smoke" [1,2]. It is now recognized as one of the major causes of stroke in adults and children worldwide [3–6]. We recently identified *RNF213* as the susceptibility gene for MMD, and the p.R4810K (rs112735431, ss179362673: G>A; herein referred to as RNF213 R4810K) polymorphism as a founder variant commonly found in East Asian (Japanese, Korean and Chinese) patients [7]. RNF213 encodes a 591 kDa protein that exhibits ATPase and ubiquitin ligase activities. Although knockdown of RNF213 in zebrafish impaired angiogenesis, the physiological and biochemical functions of RNF213, and pathological consequences of MMD associated with RNF213 R4810K remain unknown [7].

The minor allele frequency of the founder RNF213 R4810K polymorphism in the general population is estimated to be 0.43–1.36% for East Asia, equivalent to a prevalence of 0.86–2.72% for carriers. RNF213 R4810K elevates the risk of MMD by more than 100-fold in carriers [7], with approximately 15 million individuals thought to be at extremely high risk [8]. The prevalence of patients with MMD (0.01%) is much lower than that for RNF213 R4810K carriers (3%) in Japan and Korea [3,4]. We have sought to determine the triggering factors that induce MMD in RNF213 R4810K carriers. Considering the social and economic dimensions of a large high-risk population in East Asia, determination of these MMD triggering

* Corresponding author. Address: Department of Health and Environmental Sciences, Graduate School of Medicine, Kyoto University, Konoe-cho, Yoshida, Sakyo-ku, Kyoto 606-8501, Japan. Fax: +81 75 753 4458.
E-mail address: koizumi.akio.5v@kyoto-u.ac.jp (A. Koizumi).
[1] These authors contributed equally to this work.

0006-291X/$ - see front matter © 2013 Elsevier Inc. All rights reserved.
http://dx.doi.org/10.1016/j.bbrc.2013.07.004

factors is a high-priority issue. Such triggers are considered to act through RNF213 R4810K, but elucidation of these triggers has been hampered, mainly because of the lack of knowledge with respect to RNF213 R4810K pathology.

The primary aims of our study were to characterize RNF213 R4810K and the physiological functions of RNF213. To determine the pathological defects attributable to RNF213 R4810K, we tested whether vascular endothelial cells from patients with MMD have lowered angiogenic activities. Our hypothesis was based on reports of defective angiogenic activities for circulating endothelial progenitor cells in MMD patients [9]. We used induced pluripotent stem cell (iPSC) technology with the hope that it might yield useful *in vitro* disease models [10]. This approach is particularly useful for diseases in which the pathological processes have yet to be elucidated. Once an *in vitro* model has been established it is possible to reveal pathological clues about a disease; it can then be employed as a drug-screening tool, paving the way for translational research. We characterized *ex vivo* phenotypes of vascular endothelial cells differentiated from iPSCs (iPSECs) and conducted a series of *in vitro* experiments to understand the underlying mechanisms of MMD.

2. Methods

2.1. Participants

We studied three probands from three unrelated families with MMD. Diagnosis was made based on criteria from the Japanese Research Committee on MMD (Ministry of Health, Labour and Welfare, Japan) [11]. Participants consisted of six affected, or unaffected and unrelated subjects (Table 1 and Supplementary data). Genotyping revealed a AA genotype (homozygous for RNF213 R4810K) for two affected subjects, a GA genotype (heterozygous for RNF213 R4810K) in one affected and one unaffected subject, and a GG genotype (wild-type for RNF213 R4810K) for two unaffected subjects. We obtained written informed consent from all participants in this study. Our study was approved by the Institutional Ethical Review Board of Kyoto University.

2.2. Establishment of iPSECs

Dermal fibroblasts were isolated from arms and cultured. Induction of iPSCs was performed as described previously (Supplementary data) from primary fibroblasts for three MMD patients, an unaffected carrier and two controls (Table 1). We then induced the differentiation of iPSCs into vascular endothelial cells (Supplementary data). Angiogenic activity of iPSECs was assayed by tube formation. Gene expression profiles were determined using a GeneChip microarray (Human Gene 1.0 ST; Supplementary data).

Table 1
Summary of donor fibroblast information.

ID	Diagnosis	Gender	Age at onset	Age at biopsy	R4810K (G>A) of RNF213
Control 1	Healthy control	F	NA	81	GG
Control 2	Healthy control	F	NA	6	GG
Unaffected carrier	Healthy control	M	NA	36	GA
Patient 1	Familial MMD	F	10	43	GA
Patient 2	Familial MMD	F	55	63	AA
Patient 3	Familial MMD	F	50	64	AA

MMD, moyamoya disease.

2.3. Cell culture and transfection

Fibroblasts were maintained in Dulbecco's Minimal Essential Medium (DMEM; Invitrogen, Tokyo, Japan) containing 10% fetal bovine serum (FBS; Japan Bioserum, Hiroshima, Japan). The iPSCs were maintained in Primate ES medium (ReproCELL, Tokyo, Japan) and supplemented with 500 U/ml penicillin/streptomycin (Invitrogen) and 4 ng/ml recombinant human basic fibroblast growth factor (bFGF; WAKO, Tokyo, Japan) as previously reported [10,12]. Human umbilical vein endothelial cells (HUVECs; Lonza, Walkersville, MD, USA) were maintained in EGM-2 (Lonza). An mCherry-tagged wild-type RNF213 or an mCherry-tagged RNF213 R4810K was cloned into pcDNA3.1 (Invitrogen) (Supplementary data). The plasmids were introduced with an Amaxa Nucleofector Device (Lonza).

2.4. Assessment of angiogenic activity

Endothelial tube formation was assessed as described previously [13]. The iPSECs (5000 cells/well) or HUVECs (5000 cells/well or 20,000 cells/well) were seeded onto matrigel-coated (BD Biosciences, Bedford, MA, USA) 96-well plates. Cells were incubated for 12 h at 37 °C and digital images of tubes that formed were captured. For quantitation, tube area, total tube length and the number of tube branches were calculated using Image J software (National Institute of Health, USA). Parameters for assessing tube formation function were obtained from three or four independent tube formation assays.

2.5. RNA interference (RNAi)

Transfection of small interfering RNAs (siRNAs) was conducted using Dharmafect (#1 or #3; Dharmacon, Lafayette, CO, USA) following the manufacturer's recommendations. We also used Nucleofector instruments to transfect HUVECs and iPSECs according to the manufacturer's protocols. We purchased and used Securin siRNA (sc-37491; Santa Cruz Biotechnology, Santa Cruz, CA, USA), RNF213 siRNA 1 (sc-94184; Santa Cruz Biotechnology) and RNF213 siRNA 2 (s33568; Ambion, Austin, TX, USA), with control siRNA-A (sc-37007, Santa Cruz Biotechnology) and silencer select negative control #1 siRNA (Ambion) used as controls. To monitor knockdown of gene expression, real-time quantitative polymerase chain reaction (qPCR), immunostaining and/or western blotting assays were conducted.

2.6. Growth curves

Cell proliferation was assessed using colorimetric 3,4,5-dimethylthiazol-2-yl-2,5-diphenyl tetrazolium bromide (MTT) assays, which were carried out as described previously [14] unless otherwise specified. For growth curves for HUVECs in the overexpression experiment of RNF213 wild type and R4810K, at 2 days post-transfection, HUVECs were re-seeded at a density of 8×10^4 cells/3.5-mm dish. Viable cells were assessed and counted each day using trypan blue (Nacalai Tesque) exclusion.

2.7. Western blotting

We used the CelLytic M (Sigma–Aldrich, St Louis, MO, USA) cell lysis buffer containing a protease inhibitor cocktail (Nacalai Tesque). In certain cases we also used a lysis buffered comprising 50 mM Tris–HCl (pH 8.0), 1% Nonidet P-40 and 150 mM NaCl. Samples were subjected to immunoblotting using the anti-RNF213

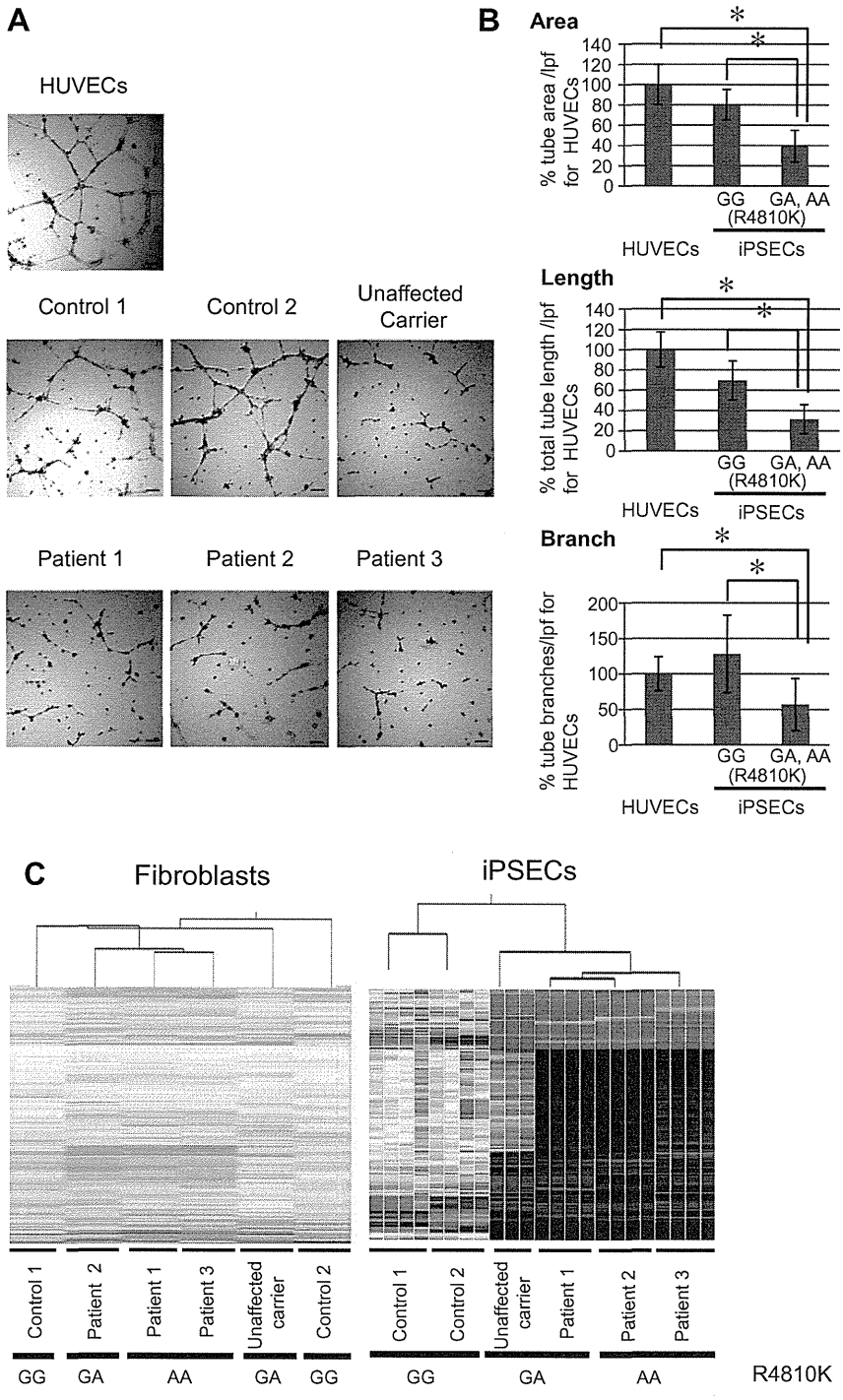

Fig. 1. Reduced angiogenic activities and differential gene expression in iPSECs. (A) Representative photomicrographs show the formation of tube-like structures in HUVECs and iPSECs from controls (GG genotype), the unaffected carrier, and patients (GA or AA genotypes). The scale bar indicates 100 μm. (B) Tube area, length and branch per low power field (lpf) were determined by matrigel assays and imaging analysis ($n = 3–4$, $^*p < 0.05$ using Student's t-test). Quantitative analysis of tube formation for iPSECs was performed between the GG genotype, and the GA and AA genotypes of p.R4810K on RNF213. HUVECs were used as a positive control. (C) Cluster analysis of fibroblasts from the control, unaffected carrier and MMD patients (single experiment) using microarrays (left panel). Cluster analysis of iPSECs from the unaffected carrier (three independent experiments), control and MMD patients (four independent experiments) using microarrays (right panel). Differentially regulated genes that were identified have been presented in Table S1.

antibody, which we generated (Supplementary data), or using anti-Securin (PTTG; Zymed, San Francisco, CA, USA), anti-β-tubulin (Sigma–Aldrich) or anti-β-actin (Abcam, Cambridge, UK) antibodies. Quantitation was conducted using Image J software.

2.8. Statistical analysis

Results are presented as the mean ± standard deviation (SD). Differences between groups were analyzed using analysis of variance (ANOVA), followed by Tukey's honestly significant difference

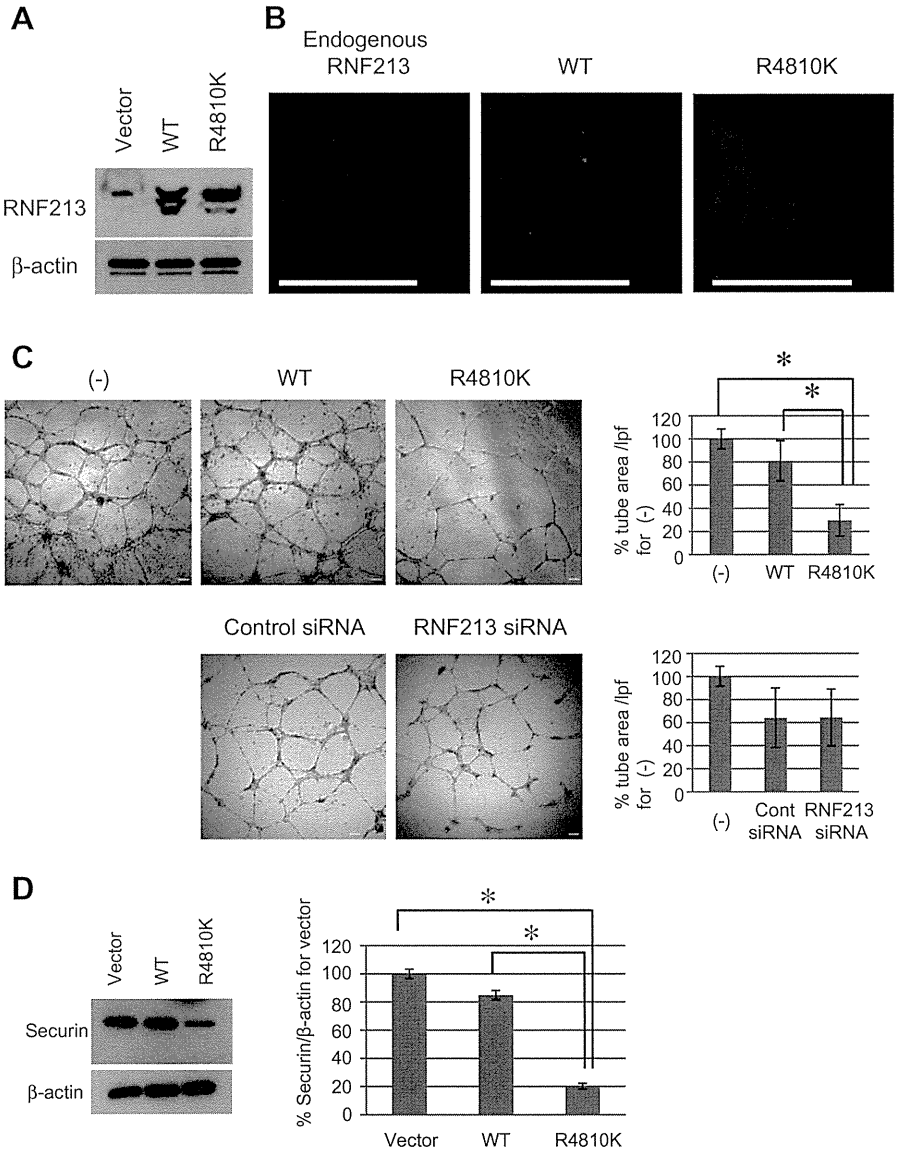

Fig. 2. Effects of RNF213 R4810K overexpression on the angiogenic activities of HUVECs. (A) Western blot analysis of endogenous and exogenous RNF213 in HUVECs. β-Actin was used as a loading control for all Western blots. (B) Subcellular localization of exogenous wild-type RNF213-mCherry (WT), RNF213 R4810K-mCherry (R4810K) and endogenous RNF213 in HUVECs. Left panel: HUVECs were stained for RNF213 (green) and DNA (blue). Middle and right panels: HUVECs transfected with RNF213-mCherry (red) were stained for tubulin (green) and DNA (blue). (C) Tube formation assays for HUVECs transfected with the RNF213 expression vector or RNF213 siRNA after 12 h of culture on matrigel. Non-transfected HUVECs (−) were used as a positive control. The scale bar indicates 100 μm. The tube areas for RNF213 overexpression ($n = 4$, $^*p < 0.05$ using Student's *t*-test) and siRNAs ($n = 3$) were quantified (right panel). Similar results were obtained for length and branch (data not shown). (D) Western blot analysis of Securin in HUVECs overexpressing wild-type RNF213 and RNF213 R4810K, with β-actin used as a loading control ($^*p < 0.01$ using Student's *t*-test). Data represents the mean of at least three independent experiments. (For interpretation of the references to color in this figure legend, the reader is referred to the web version of this article.)

test for comparisons involving more than two means (SAS Institute Inc., Cary, NC, USA). A *p*-value less than 0.05 was considered statistically significant.

3. Results

3.1. iPS cell clones

We established iPSCs from three unaffected subjects and three patients with MMD (Table 1). We used qPCR to select iPSC clones where exogenously introduced genes were repressed (Fig. S1A). Genetic identity was confirmed by genotypes of short tandem repeat (STR) markers between donor fibroblasts and iPSCs derived from these cells (Fig. S1B). All six iPSC clones showed characteristics of human embryonic stem cell morphology. They also expressed pluripotency markers, including NANOG, OCT4, SOX2, SSEA4, TRA-1-60, TRA-1-81 and alkaline phosphatase (ALP) enzymatic activity (Fig. S1C). We confirmed that there was no expression of SSEA1. The pluripotent properties of the iPSCs were confirmed by examining methylation of the OCT4 and NANOG promoter regions (Fig. S1D), and by embryoid body (EB) formation (Fig. S1E).

3.2. Reduced angiogenic activities of iPSECs in subjects with RNF213 R4810K

The iPSECs derived from iPSCs showed typical morphological features. They exhibited a cobblestone-like appearance on culture dishes, and expressed eNOS, CD31, VE-Cadherin, vWF and CD34, while iPSCs did not (Fig. S2C and D). All these features correspond

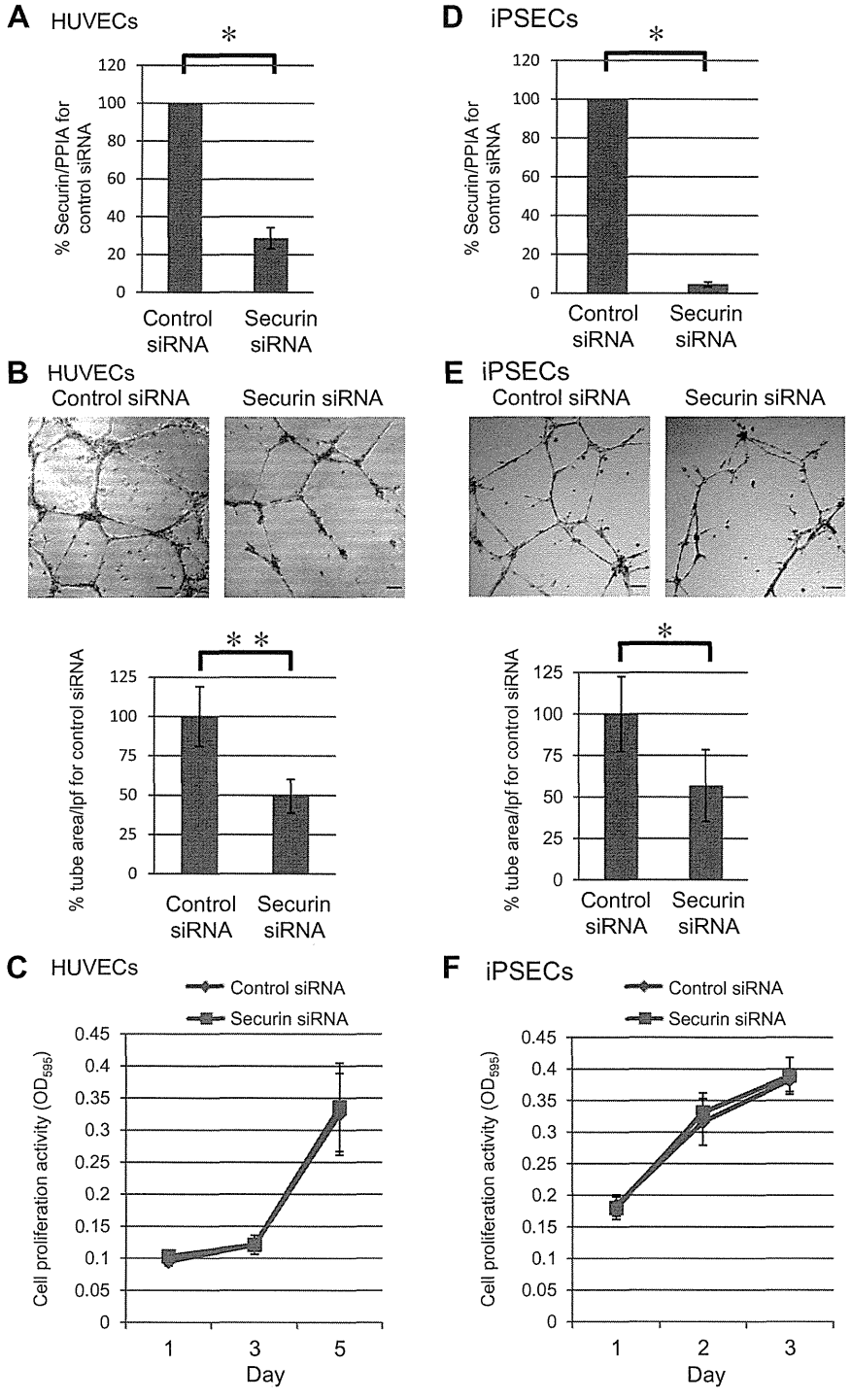

Fig. 3. The effect of depletion of Securin on angiogenic activities in HUVECs and iPSECs from a control subject. (A) RNA levels of Securin in HUVECs treated with control and Securin siRNA ($n = 3$, $^{*}p < 0.05$ using Student's t-test). (B) Representative photomicrographs (upper) and tube areas per low power field (lpf) (lower) of HUVECs treated with control and Securin siRNA ($n = 3$, $^{**}p < 0.01$ using Student's t-test). Similar results were obtained for length and branch (data not shown). The scale bar indicates 100 μm. (C) Time course of cell proliferation for HUVECs treated with control and Securin siRNA. (D) RNA levels of Securin in control iPSECs treated with control and Securin siRNA ($n = 3$, $^{*}p < 0.05$ using Student's t-test). (E) Representative photomicrographs (upper) and tube areas per lpf (lower) of control iPSECs treated with control and Securin siRNA ($n = 3$, $^{*}p < 0.05$ using Student's t-test). Similar results were obtained for length and branch (data not shown). The scale bar indicates 100 μm. (F) Time course of cell proliferation for control iPSCs treated with control and Securin siRNA.

to characteristics of vascular endothelial cells. We investigated iPSEC angiogenic activity by tube formation. The iPSECs from MMD patients and an unaffected carrier revealed significantly reduced tube areas compared with those from controls (wild-type RNF213; Fig. 1A and B and Fig. S3). Lower angiogenic activity was also confirmed by total tube length and numbers of branches (Fig. 1A and B, Fig. S3), but could not be attributed to the suppression of growth (Fig. S4).

3.3. Downregulation of mitotic phase-associated genes in iPSECs with RNF213 R4810K

To better understand whether RNF213 R4810K affects expression levels of specific genes related to reduced angiogenic activity, we used microarrays to identify differentially expressed genes in iPSECs and their parental fibroblasts. Cluster analysis of expression profiles demonstrated a clear difference for iPSECs with the RNF213 R4810K genotype (Fig. 1C).

In the iPSECs, the expression levels of 159 genes were differentially regulated by more than three-fold ($p < 0.01$). Our analysis revealed that 38 genes were up-regulated, and 121 were down-regulated (Table S1). Gene ontology analysis identified 161 significant terms ($p < 0.01$; Tables S2). Gene and ontology classifications revealed that many mitotic phase-associated genes were down-regulated (Tables S1 and S2) in iPSECs from donors with the RNF213 R4810K polymorphism. We confirmed the microarray results through qPCR assays for five genes (*Securin*, *BUB1*, *NDC80*, *PLK1* and *CDC20*) (Fig. S5).

3.4. Effects of RNF213 R4810K overexpression

Wild-type RNF213 and/or RNF213 R4810K proteins fused to the mCherry reporter (Fig. S6) were overexpressed in HUVECs (Fig. 2A and B). Plasmids were transfected into HUVECs by electroporation with gene transfer efficiencies around 72%. Overexpression of RNF213 R4810K reduced angiogenic activity in HUVECs (Fig. 2C) and significantly inhibited proliferation of HUVECs (Fig. S8). In contrast, neither overexpression nor depletion of wild-type RNF213 reduced angiogenic activity (Fig. 2C) or proliferation (Fig. S8). Localization of exogenous RNF213 R4810K was similar to that for the exogenous and endogenous wild-type RNF213, with these proteins observed in the cytoplasm around the nucleus (Fig. 2B). Overexpression of RNF213 R4810K significantly down-regulated the expression of Securin ($p < 0.01$; Fig. 2D), while overexpression of wild-type RNF213 had little effect on Securin.

3.5. Depletion of Securin affects angiogenic activities of HUVECs and iPSECs

Securin induces angiogenesis, and is an inhibitor of premature sister chromatid separation [15]. Depletion of Securin induces severe defects in cell migration by lowered microtubule nucleation [16], which results in lowered angiogenic activity. We then examined the effects of RNAi-mediated depletion of Securin on tube formation and proliferation using HUVECs and iPSECs carrying wild alleles. RNAi knockdown of Securin was shown to impair tube formation without inhibiting proliferation in both HUVECs (Fig. 3A–C) and iPSECs (Fig. 3D–F).

4. Discussion

In this study, we successfully differentiated iPSECs from the iPSCs of MMD patients and carriers harboring GA or AA genotypes of RNF213 R4810K. The iPSECs with GA or AA genotypes replicated lowered angiogenic activity for circulating endothelial progenitor cells in MMD patients [9]. To the best of our knowledge, we are the first to report the generation of MMD-specific iPSCs that are able to differentiate into iPSECs, which can then be used as an *in vitro* MMD model.

Reduced angiogenic activity was consistently observed in iPSECs from subjects that had RNF213 R4810K, and in HUVECs overexpressing RNF213 R4810K. Because gene expression of Securin, which is known to require for angiogenesis [15], was suppressed in iPSECs carrying RNF213 R4810K, we investigated the effects of RNAi-mediated knockdown of Securin on tube formation in HUVECs and iPSECs. Depletion of Securin inhibited tube formation consistently without inhibition of proliferation as we observed lowered tube formation of iPSECs from patients and the carrier. This indicated to us that reduced expression of Securin per se is responsible for lowered angiogenic activity. Because cell migration is known to be impaired when Securin is depleted [16], we postulate that the defect in migration might occur in iPSECs, thereby reducing angiogenic activity.

We did not investigate abnormalities of vascular smooth muscle cells (VSMCs), which could be considered a limitation of our work. A major pathological finding in MMD is the excessive proliferation of VSMCs. The interactions between ECs and VSMCs are known to play key roles in vascular structure and function of vessels. VSMC migration, proliferation, and differentiation are critical processes involved in intimal hyperplasia and are under regulation by endothelial cells [17]. We postulate that there is a defect in the crosstalk between ECs and VSMCs in patients.

Many mitosis-related genes were downregulated by RNF213 R4810K. We focused on Securin and determined that its downregulation may play a substantial role in lowered angiogenic activity of iPSECs from patients with MMD. However, in the present study, we did not investigate the effects of other downregulated genes. Furthermore, we did not investigate the mechanisms of Securin downregulation in iPSECs from MMD patients. Further studies are needed to substantiate the roles of RNF213 R4810K in downregulation of mitotic associated genes.

In conclusion, we observed that iPSECs from MMD patients had impaired angiogenic functions. RNF213 R4810K manifests as defects in angiogenesis by the downregulation of Securin expression. The resulting defects in angiogenesis are considered risk factors for MMD patients. Furthermore, our study demonstrated that iPSECs can serve as an *in vitro* MMD model, as they express a useful benchmark phenotype for high throughput screening, which can be applied to drug development and discovering MMD triggers.

Funding sources

This work was supported by grants from the Ministry of Education, Culture, Sports, Science and Technology of Japan (Nos. 17109007 and 22249020 to Dr. Koizumi). This research was partially supported by the Japan Society for the Promotion of Science through its Funding Program for World-Leading Innovative R&D on Science and Technology (FIRST Program to Dr. Osafune).

Acknowledgments

We are grateful to Drs. Wanyang Liu, Shanika Nanayakkara, and STMLD Senevirathna (Kyoto University Graduate School of Medicine) for their technical support.

Appendix A. Supplementary data

Supplementary data associated with this article can be found, in the online version, at http://dx.doi.org/10.1016/j.bbrc.2013.07.004.

References

[1] J. Suzuki, A. Takaku, Cerebrovascular "moyamoya" disease. Disease showing abnormal net-like vessels in base of brain, Arch. Neurol. 20 (1969) 288–299.
[2] K. Takeuchi, K. Shimizu, Hypogenesis of bilateral internal carotid arteries, Brain Nerve 9 (1957) 37–43.
[3] S. Kuroda, K. Houkin, Moyamoya disease: current concepts and future perspectives, Lancet Neurol. 7 (2008) 1056–1066.
[4] W. Miao, P.L. Zhao, Y.S. Zhang, H.Y. Liu, Y. Chang, J. Ma, Q.J. Huang, Z.X. Lou, Epidemiological and clinical features of moyamoya disease in Nanjing, China, Clin. Neurol. Neurosurg. 112 (2010) 199–203.

[5] R.M. Scott, E.R. Smith, Moyamoya disease and moyamoya syndrome, N. Engl. J. Med. 360 (2009) 1226–1237.
[6] A. Veeravagu, R. Guzman, C.G. Patil, L.C. Hou, M. Lee, G.K. Steinberg, Moyamoya disease in pediatric patients: outcomes of neurosurgical interventions, Neurosurg. Focus 24 (2008) E16.
[7] W. Liu, D. Morito, S. Takashima, Y. Mineharu, H. Kobayashi, T. Hitomi, H. Hashikata, N. Matsuura, S. Yamazaki, A. Toyoda, K. Kikuta, Y. Takagi, K.H. Harada, A. Fujiyama, R. Herzig, B. Krischek, L. Zou, J.E. Kim, M. Kitakaze, S. Miyamoto, K. Nagata, N. Hashimoto, A. Koizumi, Identification of RNF213 as a susceptibility gene for moyamoya disease and its possible role in vascular development, PLoS ONE 6 (2011) e22542.
[8] W. Liu, T. Hitomi, H. Kobayashi, K.H. Harada, A. Koizumi, Distribution of moyamoya disease susceptibility polymorphism p.R4810K in RNF213 in East and Southeast Asian Populations, Neurol. Med. Chir. 52 (2012) 299–303.
[9] J.H. Kim, J.H. Jung, J.H. Phi, H.S. Kang, J.E. Kim, J.H. Chae, S.J. Kim, Y.H. Kim, Y.Y. Kim, B.K. Cho, K.C. Wang, S.K. Kim, Decreased level and defective function of circulating endothelial progenitor cells in children with moyamoya disease, J. Neurosci. Res. 88 (2010) 510–518.
[10] K. Takahashi, K. Tanabe, M. Ohnuki, M. Narita, T. Ichisaka, K. Tomoda, S. Yamanaka, Induction of pluripotent stem cells from adult human fibroblasts by defined factors, Cell 131 (2007) 861–872.
[11] M. Fukui, Guidelines for the diagnosis and treatment of spontaneous occlusion of the circle of Willis ('moyamoya' disease). Research Committee on Spontaneous Occlusion of the Circle of Willis (Moyamoya Disease) of the Ministry of Health and Welfare, Japan, Clin. Neurol. Neurosurg. 99 (Suppl. 2) (1997) S238–S240.
[12] K. Amps, P.W. Andrews, G. Anyfantis, L. Armstrong, S. Avery, H. Baharvand, J. Baker, D. Baker, M.B. Munoz, S. Beil, N. Benvenisty, D. Ben-Yosef, J.C. Biancotti, A. Bosman, R.M. Brena, D. Brison, G. Caisander, M.V. Camarasa, J. Chen, E. Chiao, Y.M. Choi, A.B. Choo, D. Collins, A. Colman, J.M. Crook, G.Q. Daley, A. Dalton, P.A. De Sousa, C. Denning, J. Downie, P. Dvorak, K.D. Montgomery, A. Feki, A. Ford, V. Fox, A.M. Fraga, T. Frumkin, L. Ge, P.J. Gokhale, T. Golan-Lev, H. Gourabi, M. Gropp, G. Lu, A. Hampl, K. Harron, L. Healy, W. Herath, F. Holm, O. Hovatta, J. Hyllner, M.S. Inamdar, A.K. Irwanto, T. Ishii, M. Jaconi, Y. Jin, S. Kimber, S. Kiselev, B.B. Knowles, O. Kopper, V. Kukharenko, A. Kuliev, M.A. Lagarkova, P.W. Laird, M. Lako, A.L. Laslett, N. Lavon, D.R. Lee, J.E. Lee, C. Li, L.S. Lim, T.E. Ludwig, Y. Ma, E. Maltby, I. Mateizel, Y. Mayshar, M. Mileikovsky, S.L. Minger, T. Miyazaki, S.Y. Moon, H. Moore, C. Mummery, A. Nagy, N. Nakatsuji, K. Narwani, S.K. Oh, C. Olson, T. Otonkoski, F. Pan, I.H. Park, S. Pells, M.F. Pera, L.V. Pereira, O. Qi, G.S. Raj, B. Reubinoff, A. Robins, P. Robson, J. Rossant, G.H. Salekdeh, T.C. Schulz, et al., Screening ethnically diverse human embryonic stem cells identifies a chromosome 20 minimal amplicon conferring growth advantage, Nat. Biotechnol. 29 (2011) 1132–1144.
[13] M. Potente, L. Ghaeni, D. Baldessari, R. Mostoslavsky, L. Rossig, F. Dequiedt, J. Haendeler, M. Mione, E. Dejana, F.W. Alt, A.M. Zeiher, S. Dimmeler, SIRT1 controls endothelial angiogenic functions during vascular growth, Genes Dev. 21 (2007) 2644–2658.
[14] T. Mosmann, Rapid colorimetric assay for cellular growth and survival: application to proliferation and cytotoxicity assays, J. Immunol. Methods 65 (1983) 55–63.
[15] H. Ishikawa, A.P. Heaney, R. Yu, G.A. Horwitz, S. Melmed, Human pituitary tumor-transforming gene induces angiogenesis, J. Clin. Endocrinol. Metab. 86 (2001) 867–874.
[16] M.A. Moreno-Mateos, A.G. Espina, B. Torres, M.M. Gamez del Estal, A. Romero-Franco, R.M. Rios, J.A. Pintor-Toro, PTTG1/securin modulates microtubule nucleation and cell migration, Mol. Biol. Cell 22 (2011) 4302–4311.
[17] F. Milliat, A. Francois, M. Isoir, E. Deutsch, R. Tamarat, G. Tarlet, A. Atfi, P. Validire, J. Bourhis, J.C. Sabourin, M. Benderitter, Influence of endothelial cells on vascular smooth muscle cells phenotype after irradiation: implication in radiation-induced vascular damages, Am. J. Pathol. 169 (2006) 1484–1495.

Original Article

Adrenal reserve function after unilateral adrenalectomy in patients with primary aldosteronism

Kyoko Honda[a], Masakatsu Sone[a], Naohisa Tamura[a], Takuhiro Sonoyama[a], Daisuke Taura[a], Katsutoshi Kojima[a], Yorihide Fukuda[a], Shiro Tanaka[b], Shinji Yasuno[c], Toshihito Fujii[a], Hideyuki Kinoshita[a], Hiroyuki Ariyasu[a], Naotetsu Kanamoto[a], Masako Miura[a], Akihiro Yasoda[a], Hiroshi Arai[a], Kenji Ueshima[c], and Kazuwa Nakao[a]

Objective: After unilateral adrenalectomy (uADX) in patients with a unilateral aldosterone-producing adenoma (APA), the remaining contralateral adrenal gland is generally considered sufficient to support life. However, few studies have compared adrenal reserve function before and after uADX. Therefore, we closely evaluated adrenal cortisol secretory function before and after uADX in patients with unilateral APA.

Methods: Patients who were diagnosed with APA and underwent uADX for unilateral APA were initially included in this study. Patients with subclinical Cushing's syndrome (SCS) or Cushing's syndrome were excluded on suspicion of autonomous cortisol secretion. Fourteen patients were finally evaluated. Morning basal serum cortisol and plasma adrenocorticotropin hormone (ACTH) levels were measured, and ACTH stimulation tests under 1-mg dexamethasone suppression (dex-ACTH test) were performed before and after uADX.

Results: No patient developed clinical adrenal insufficiency. Basal cortisol levels were not significantly different before and after uADX. However, basal ACTH levels were significantly elevated after uADX. In addition, peak cortisol levels on the dex-ACTH test decreased in all patients after uADX. The peak cortisol level after uADX was 86.6 (81.4–92.4)% of the level before uADX.

Conclusion: The adrenal cortisol secretory response to ACTH stimulation is mildly reduced after uADX in patients with unilateral APA without SCS or Cushing's syndrome, although their basal cortisol level is sustained by elevated ACTH. These data will be important as a point of discussion when patients with unilateral APA consider either uADX or specific pharmacotherapy as treatment options.

Keywords: adrenal function, adrenal gland, adrenal insufficiency, cortisol, primary aldosteronism, unilateral adrenalectomy

Abbreviations: A/C, aldosterone-to-cortisol ratio; ACTH, adrenocorticotropin hormone; APA, aldosterone-producing adenoma; ARR, aldosterone-to-renin ratio; AUC, area under the curve; AVS, adrenal venous sampling; dex-ACTH test, ACTH stimulation test under 1-mg dexamethasone suppression; HPA, hypothalamic-pituitary-adrenal; PAC, plasma aldosterone concentration; PRA, plasma renin activity; SCS, subclinical Cushing's syndrome; uADX, unilateral adrenalectomy

INTRODUCTION

Primary aldosteronism is a group of disorders in which aldosterone production is inappropriately high with suppression of plasma renin. Such inappropriate aldosterone production causes sodium retention and potassium excretion that, if prolonged and severe, may lead to hypertension and hypokalemia. The incidence of primary aldosteronism in patients with hypertension has been considered to be less than 1%, but recent studies have reported a much higher primary aldosteronism prevalence nearing 10% [1–6]. Primary aldosteronism is important not only because of its prevalence, but also because patients with primary aldosteronism have higher cardiovascular morbidity and mortality than age-matched and sex-matched patients with essential hypertension and the same degree of blood pressure elevation [7,8]. Primary aldosteronism is caused by unilateral primary aldosteronism, including unilateral aldosterone-producing adenoma (APA), unilateral adrenal hyperplasia (UAH), unilateral multiple micronodules (UMN), and aldosterone-producing carcinoma (APC), or by bilateral primary aldosteronism, including idiopathic hyperaldosteronism (IHA), bilateral APA, and glucocorticoid suppressive hyperaldosteronism (GSH) [1–6]. Among them, APA and IHA account for more than 95% of all primary aldosteronism cases. Unilateral adrenalectomy (uADX) is generally

Journal of Hypertension 2013, 31:2010–2017

[a]Department of Medicine and Clinical Science, Kyoto University Graduate School of Medicine, [b]Department of Clinical Trial Design & Management, Translational Research Center, Kyoto University Hospital and [c]EBM Research Center, Kyoto University Graduate School of Medicine, Kyoto, Japan

Correspondence to Masakatsu Sone, MD, PhD, Department of Medicine and Clinical Science, Kyoto University Graduate School of Medicine, 54 Shogoin-Kawahara-cho, Sakyo-ku, Kyoto 606–8507, Japan. Tel: +81 75 751 3170; fax: +81 75 771 9452; e-mail: sonemasa@kuhp.kyoto-u.ac.jp

Received 21 January 2013 **Revised** 2 April 2013 **Accepted** 16 May 2013

J Hypertens 31:2010–2017

DOI:10.1097/HJH.0b013e3283635789

recommended for patients with unilateral APA, whereas pharmacotherapy with mineralocorticoid receptor antagonists is another therapeutic option. uADX in patients with unilateral APA normalizes hypokalemia, improves hypertension in almost all patients, and fully controls hypertension in approximately 30–72% of patients [2,9].

It is generally considered that even after uADX, the remaining contralateral adrenal gland can sufficiently support life because the adrenal gland is critical for survival and may have a large amount of reserve function for maintenance of homeostasis. A few studies have examined adrenal function or cortisol secretion after uADX [10,11]. For example, Gordon *et al.* [10] reported reduced plasma levels of cortisol, aldosterone, and catecholamines following uADX for unilateral primary aldosteronism. However, in these earlier reports, only the basal cortisol levels were compared before and after uADX. Meanwhile, some patients can develop relative adrenal insufficiency in extreme illness even if they have two healthy adrenal glands and their baseline cortisol and adrenocorticotropin hormone (ACTH) levels are within the normal range [12,13]. Therefore, patients with one adrenal gland after uADX may be more susceptible to relative adrenal insufficiency compared with patients with two healthy adrenal glands in such a situation, although no clinical studies have proven this. Before irrevocable surgical intervention, it is preferable for both doctors and patients to have precise data about changes in adrenal reserve function by the intervention. Although we cannot predict the risk of relative adrenal insufficiency, evaluation of the basal cortisol level alone is not enough to properly predict the adrenocortical reserve function. The ACTH stimulation test is widely used as a simple method to identify adrenocortical hyporesponsiveness. The ACTH stimulation test assesses the stress response of the adrenal gland by measuring the adrenal cortisol response to synthetic ACTH. Thus, in this study, we compared the cortisol response to ACTH by performing an ACTH stimulation test before and after uADX.

In addition, because APA is sometimes accompanied by subclinical Cushing's syndrome (SCS) or Cushing's syndrome, their exclusion is important for accurate evaluation.

Therefore, in this study, we investigated adrenocortisol function by comparing basal serum cortisol, plasma ACTH levels, and the cortisol response to ACTH on the ACTH stimulation test under 1-mg dexamethasone suppression (dex-ACTH test) before and after uADX in patients with APA without SCS or Cushing's syndrome. The objective of this study was to evaluate residual adrenal cortisol secretory function after uADX in these patients.

METHODS

We retrospectively analyzed the patients with APA who were admitted to the Department of Endocrinology and Metabolism of Kyoto University Hospital, Kyoto, Japan, and underwent uADX over the past 6 years. The study was approved by the Kyoto University Graduate School and Faculty of Medicine Ethics Committee and was conducted in accordance with the principles of the Declaration of Helsinki.

Diagnosis of primary aldosteronism

Hypertensive patients who were referred to our hospital were initially screened by determining their aldosterone-to-renin ratio [ARR; the ratio of plasma aldosterone concentration (PAC) to plasma renin activity (PRA)]. A positive screening was defined as an ARR over 555 pmol/l per ng/ml per h (>20 ng/dl per ng/ml per h). PRA and PAC were measured in blood samples obtained after 30 min of rest in a supine position in the morning. All antihypertensive drugs with the exception of calcium channel blockers and α blockers were stopped at least 4 weeks before the measurement of PRA and PAC [14]. Patients with hypokalemia (i.e. serum potassium level less than 3.5 mmol/l) were allowed to take oral potassium supplementation.

Confirmatory tests for primary aldosteronism

We performed the captopril challenge test and the saline infusion test to confirm the diagnosis of primary aldosteronism in this study. In the captopril challenge test, an ARR of at least 555 pmol/l per ng/ml per h (20 ng/dl per ng/ml per h) 60 min after administration of 50 mg of captopril was considered positive for primary aldosteronism. For the saline infusion test, a PAC of at least166 pmol/l (6.0 ng/dl) after infusion of 2 l of 0.9% saline was considered positive for primary aldosteronism. Patients who showed positive captopril challenge test results and/or positive saline infusion test results were diagnosed with primary aldosteronism in this study [15].

Diagnosis of aldosterone-producing adenoma

Patients with confirmed primary aldosteronism underwent subtype diagnosis prior to surgery. Adrenal CT scanning was performed for initial localization. The definitive test for subtype diagnosis was adrenal venous sampling (AVS) [16]. AVS was performed by expert radiologists with ACTH stimulation as previously described [17]. Adrenal vein cannulation was considered successful if the adrenal vein/inferior vena cava cortisol gradient (selectivity index) was more than 3.0. We considered lateralization to be present when the aldosterone-to-cortisol ratio (A/C) from one adrenal gland was more than three times the ratio from the other adrenal gland (lateralization ratio) and the A/C in the contralateral adrenal vein was lower than the A/C in the vena cava (contralateral ratio).

Diagnosis of APA required the following: diagnosis of primary aldosteronism by the captopril challenge test and/or saline infusion test, lateralization of aldosterone secretion at AVS, pathological evidence of adrenal adenoma in the adrenal gland with aldosterone hypersecretion, and normalization of PAC after uADX.

Exclusion criteria

The following patients were excluded from this study: patients with autonomous cortisol secretion [i.e., plasma cortisol level of ≥49.7 nmol/l (1.8 μg/dl) after overnight 1-mg dexamethasone suppression] with suspicion of autonomous cortisol secretion, such as that induced by SCS or Cushing's syndrome [18–21] and patients with incomplete data collection (i.e. patients for whom the dex-ACTH test was not performed before or after surgery).

Blood sampling and adrenocorticotropin hormone stimulation test under 1-mg dexamethasone suppression (dex-ACTH test)

Before and 2 weeks after uADX, blood samples were collected between 0800 and 0900 h after the patients had maintained a supine position for 30 min to measure the basal serum cortisol and plasma ACTH levels. The dex-ACTH test was also performed before and 2 weeks after uADX as follows: 1 mg of dexamethasone was orally administered at 2300 h the night before ACTH injection. At 0900 h the following morning, 250 μg of synthetic ACTH was intravenously injected, and blood samples were collected every 30 min until 120 min after the injection of ACTH. Serum cortisol levels were measured at each time point. The area under the curve (AUC) of the dex-ACTH test was calculated by adding the areas under the cortisol-time curve for the intervals 0–30, 30–60, 60–90, and 90–120 min. This test was repeated 1 year after uADX in six patients who requested reassessment of their adrenocortical reserve function after uADX for a longer duration.

Blood pressure measurement

Blood pressures were measured in a quiet, warm room with patients in a seated position with the arm held at heart level. The blood pressures listed in Table 1 were those obtained the morning after hospitalization.

Measurements of hormones

PRA was measured using a commercially available radioimmunoassay (Renin RIAbeads; TFB Factories Ltd, Tokyo, Japan). PAC was measured by radioimmunoassay with a commercial kit (Spec-S Aldosterone Kit; TFB Factories Ltd). Cortisol was measured by an enzyme immunoassay with the E-test TOSOH II (Cortisol) (Tosoh Corporation, Tokyo, Japan) on an automated immunoassay analyzer (AIA-1800; Eiken Chemical Co., Ltd., Tokyo, Japan). ACTH was measured using a commercially available electrochemiluminescence immunoassay (ECLusys ACTH; Roche Diagnostics Corporation, Tokyo, Japan).

Statistical analysis

All data were expressed as medians with the interquartile range (IQR). Data obtained before and after uADX were compared using the Wilcoxon signed rank test. A $P < 0.05$ was considered to be statistically significant. All statistical analyses were performed using SAS version 9.2 (SAS Institute, Cary, North Carolina, USA).

RESULTS

Patients

Twenty-nine consecutive patients underwent operations for unilateral APA from 2006 to 2012 in our hospital. Among them, seven patients with serum cortisol levels more than or equal to 49.7 nmol/l (≥1.8 μg/dl) after overnight 1-mg dexamethasone suppression were excluded from this study because of a suspicion of autonomous cortisol secretion. Another eight patients were excluded because of incomplete data collection. As a result, 14 patients were included in this study. The clinical characteristics of the 14 patients are shown in Table 1. No patients developed clinically

TABLE 1. Clinical characteristics of patients with unilateral aldosterone-producing adenoma before and 2 weeks after unilateral adrenalectomy

	Before	2 weeks after	*P* before vs. 2 weeks after
Number of patients	14		
Sex (male : female)	5 : 9		
Age, years	47.5 (40.5–57.5)		
Number of patients with family history of more than one first-degree relative with hypertension	1		
Number of patients with a duration of hypertension of >5 years	6		
Number of patients using antihypertensive drugs	12	2	
SBP (mmHg)	128.5 (122.8–136.0)	115.5 (105.5–123.8)	<0.01
DBP (mmHg)	85.5 (80.3–94.5)	76.5 (74.0–86.3)	<0.05
Estimated GFR (ml/min per 1.73 m^2)	73.1 (66.5–82.8)	73.1 (67.0–80.2)	NS
Serum potassium (mmol/l)	3.3 (3.0–3.6)	4.3 (4.1–4.5)	<0.01
Oral potassium supplementation (mmol/day)	24 (16–32)	0	
Urinary aldosterone (nmol/day)	41.8 (36.7–49.9)	3.9 (2.7–6.8)	<0.01
PAC (pmol/l)	605.2 (486.1–952.9)	166.2 (128.8–190.4)	<0.01
PRA (ng/ml per h)	0.1 (0.1–0.4)	0.7 (0.4–1.2)	<0.01
PAC/PRA (pmol/l per ng/ml per h)	4321.2 (2200.1–8614.7)	214.7 (111.1–361.8)	<0.01
Cortisol (nmol/l)	303.5 (272.5–364.2)	296.6 (270.4–357.3)	NS
ACTH (pmol/l)	4.4 (2.9–5.8)	7.0 (4.8–10.5)	<0.01
Percentage of eosinophils (%)	2.8 (2.3–4.1)	6.0 (4.9–7.9)	<0.01
Laterality of adenoma (left : right)	7 : 7		
Tumor diameter (mm)	14.5 (12.0–19.3)		

ACTH, adrenocorticotropin hormone; NS, not significant; PAC, plasma aldosterone concentration; PRA, plasma renin activity. Values are medians (interquartile range). Normal values: urinary aldosterone, <27.7 nmol/24 h; PAC, 82.8–439.9 pmol/l; PRA, 0.2–2.7 ng/ml per h; ACTH, 1.5–12.3 pmol/l; cortisol: 138.0–579.4 nmol/l. For PAC, 1 ng/dl converts to 27.7 pmol/l in the International System of Units (SI units); for urine aldosterone, 1 μg/24 h converts to 2.77 nmol/24 h in SI units; for ACTH, 1 pg/ml converts to 0.22 pmol/l in SI units; and for cortisol, 1 μg/dl converts to 27.59 nmol/l in SI units.

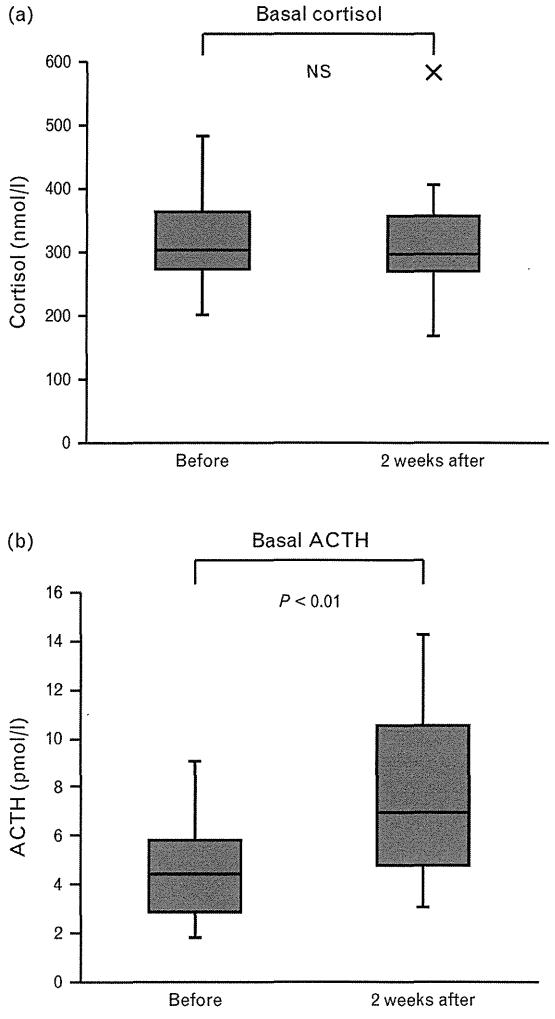

FIGURE 1 Serum cortisol (a) and plasma ACTH (b) levels before and 2 weeks after unilateral adrenalectomy in 14 patients. ACTH, adrenocorticotropin hormone; NS, not significant.

apparent adrenal insufficiency. The serum potassium level normalized after uADX in all 14 patients. Before uADX, all 14 patients had hypertension and 12 of them were prescribed antihypertensive agents. Two weeks after uADX, the blood pressure normalized without medication in 12 patients and the antihypertensive drugs were reduced in the remaining two patients. Six months after uADX, the blood pressure of 10 of the 12 patients remained normal without medication, but the blood pressure in the remaining two patients rose again. Medication was restarted in these two patients, although the dose was lower than that administered preoperatively. Therefore, we consider that hypertension was cured in 10 of the 14 patients and improved in the remaining four patients, 6 months after uADX.

Basal adrenocorticotropin hormone and cortisol levels

The basal cortisol levels before and after uADX were 303.5 (272.5–364.2) and 296.6 (270.4–357.3) nmol/l, respectively. The basal ACTH levels before and after uADX were 4.4 (2.9–5.8) and 7.0 (4.8–10.5) pmol/l, respectively. The basal cortisol levels were within the normal range in all patients and were not significantly different before and after uADX ($P=0.706$) (Fig. 1a). Although the plasma ACTH levels were also within the normal range, they were significantly higher after uADX than before ($P<0.01$) (Fig. 1b).

Adrenocorticotropin hormone stimulation test under 1-mg dexamethasone suppression (dex-ACTH test)

On the dex-ACTH test, the peak cortisol level in response to 250 μg of ACTH was lower after uADX than before uADX in all patients. The peak cortisol level was mildly but significantly decreased after uADX to 86.6 (81.4–92.4)% of the level before uADX [535.2 (497.3–575.9) vs. 649.7 (604.2–700.8) nmol/l; $P<0.01$] (Table 2, Fig. 2a). The cortisol AUC was also significantly decreased after uADX to 82.6 (79.0–91.9)% of that before uADX (46703.0 [43888.8–51017.4] vs. 58021.8 [55052.4–60867.0] nmol/l/120 min; $P<0.01$) (Table 2, Fig. 2b).

DISCUSSION

In patients with SCS or Cushing's syndrome, autonomous cortisol hypersecretion from the cortisol-producing adenoma suppresses the hypothalamic-pituitary-adrenal (HPA) axis and cortisol secretion from the healthy contralateral adrenal cortex. Therefore, adrenal insufficiency

TABLE 2. Serum cortisol levels (nmol/l) and cortisol area under the curve (nmol/l per 120 min) during an adrenocorticotropin hormone stimulation test under 1-mg dexamethasone suppression before and 2 weeks after unilateral adrenalectomy in the 14 patients with unilateral aldosterone-producing adenoma

	Before	2 weeks after	*P* before vs. 2 weeks after	Ratio: (2 weeks after)/(before) (%)	Decrease in parameters by uADX (%)
30 min	416.6 (376.6–446.3)	333.8 (310.4–386.3)	<0.01	83.0 (78.1–93.2)	17.0 (6.8–21.9)
60 min	561.5 (528.3–589.0)	430.4 (409.0–483.5)	<0.01	80.3 (77.3–89.9)	19.7 (10.1–22.7)
90 min	620.8 (577.3–653.2)	507.7 (478.7–537.3)	<0.01	83.7 (80.0–92.1)	16.3 (7.9–20.0)
120 min	624.9 (595.9–694.6)	532.5 (495.9–575.9)	<0.01	87.5 (78.6–93.4)	12.5 (6.6–21.4)
Peak	649.7 (604.2–700.8)	535.2 (497.3–575.9)	<0.01	86.6 (81.4–92.4)	13.4 (7.6–18.6)
AUC	58021.8 (55052.4–60867.0)	46703.0 (43888.8–51017.4)	<0.01	82.6 (79.0–91.9)	17.4 (8.1–21.0)

uADX, unilateral adrenalectomy; AUC, area under the curve. Values are medians (interquartile range).

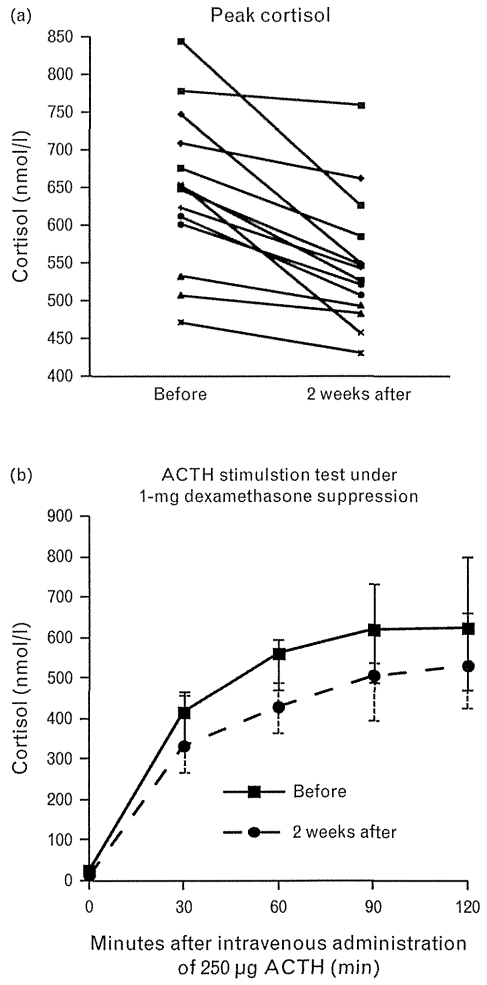

FIGURE 2 (a) Peak cortisol levels on the ACTH stimulation test under 1-mg dexamethasone suppression performed before and 2 weeks after unilateral adrenalectomy in 14 patients. (b) Cortisol levels at 0, 30, 60, 90, and 120 min after intravenous administration of 250 μg ACTH. Results are expressed as individual values (a) or medians with the interquartile range (IQR) (b). ACTH, adrenocorticotropin hormone.

often occurs after uADX. However, in patients with primary aldosteronism without SCS or Cushing's syndrome, the HPA axis is not suppressed, and cortisol secretion from the healthy contralateral normal adrenal cortex is maintained. Therefore, it is generally considered that adrenal insufficiency does not occur after uADX in patients with primary aldosteronism without SCS or Cushing's syndrome.

Generally, basal cortisol levels are measured to assess adrenal function. However, the basal cortisol level is markedly variable according to blood sampling conditions, and it is difficult to evaluate small differences in data obtained with single blood samplings. In addition, evaluation of the basal cortisol levels alone is not enough to properly predict the adrenocortical reserve function. To overcome these limitations, we performed the dex-ACTH test to precisely evaluate adrenal reserve function after uADX. The ACTH stimulation test is generally used to evaluate adrenal reserve function [22–24], although it is sometimes used to confirm primary aldosteronism by measuring the plasma aldosterone concentration [25,26]. The ACTH stimulation test following 1-mg dexamethasone suppression (i.e., dex-ACTH test) is also useful to evaluate adrenal reserve function [27]. Administration of 1 mg dexamethasone at 2300 h suppresses the HPA axis on the following morning and can eliminate the effect of endogenous ACTH. Subsequent administration of a fixed and large amount of ACTH permits evaluation of adrenal responsiveness to the stimulation (i.e. the adrenal reserve function).

In the present study, we found that basal plasma ACTH levels after uADX were significantly higher than those before uADX. The basal serum cortisol levels were within the normal range in all patients and were not significantly different before and after uADX. In addition, on the dex-ACTH test, the peak cortisol level and the cortisol AUC in response to 250 μg of ACTH were mildly but significantly decreased after uADX, which indicates that adrenal responsiveness to ACTH stimulation decreased after uADX. These results suggest that the adrenal reserve function is mildly reduced after uADX but that the basal cortisol secretion is preserved by the increased basal plasma ACTH levels [28].

The peak cortisol level in response to ACTH was significantly lower after uADX than before uADX ($P < 0.01$) (Table 2). However, the cortisol responsiveness to ACTH stimulation after uADX was maintained at 86.6 (81.4–92.4)% of that before uADX. Among all 14 patients after uADX, four had peak cortisol levels of 415–500 nmol/l, six had peak cortisol levels of 500–550 nmol/l, and four had peak cortisol levels of more than 550 nmol/l. None of the 14 patients had a peak cortisol level of less than 415 nmol/l on the dex-ACTH test, and we supposed that no apparent adrenal insufficiency was diagnosed in these patients [22–24]. This may explain why clinically apparent adrenal insufficiency did not occur in our patients after uADX. Our results provide important evidence that reassures and supports the current clinical opinion of uADX as a well tolerated procedure in primary aldosteronism with minimal risk of significant adrenal insufficiency. On the other hand, our results indicate that adrenal reserve function after uADX is not the same as that before uADX. The change in adrenal reserve function by uADX may result in changes to the patient's physical potentials that are difficult to detect during general medical examinations; such changes may include physical stress endurance, or maximum physical ability in sports.

Two weeks after uADX, the blood pressure normalized without medication in 12 of the 14 patients; however, no patients developed hypotension. Furthermore, hyponatremia and hyperkalemia were not observed after uADX. However, the percentage of eosinophils increased significantly after uADX ($P < 0.01$) (Table 1, Supplementary Table 1, Supplemental Digital Content 1, http://links.lww.com/HJH/A270). The amount of circulating eosinophils is often used as a marker for the biological effect of glucocorticoids and adrenocortical function [29,30]. Therefore, the increase in eosinophils might represent a slight reduction in adrenocortical reserve function, although clinically significant adrenal insufficiency did not occur in these patients.

Although the number of cases included in this study was not large, the sample size was sufficient to detect elevated

TABLE 3. Adrenal function before, 2 weeks after, and 1 year after unilateral adrenalectomy in six patients with unilateral aldosterone-producing adenoma

	Before	2 weeks after	*P* before vs. 2 weeks after	1 year after	*P* before vs. 1 year after
Number of patients	6				
Sex (male : female)	3 : 3				
Age (years)	52.0 (47.3–57.5)				
Basal cortisol (nmol/l)	291.1 (229.0–371.8)	280.0 (247.6–320.7)	NS	230.4 (218.7–320.7)	NS
Basal ACTH (pmol/l)	3.4 (2.7–5.1)	5.8 (4.4–7.3)	<0.05	5.9 (3.8–7.1)	<0.05
Peak cortisol (nmol/l)	663.5 (622.2–752.5)	555.9 (522.8–615.9)	<0.05	573.9 (547.0–658.7)	<0.05
Cortisol AUC (10^4 nmol/l per 120 min)	5.920 (5.580–6.888)	4.933 (4.466–5.785)	<0.05	5.078 (4.693–5.925)	<0.05
Percentage of eosinophils (%)	2.8 (2.6–3.0)	7.0 (5.3–7.9)	<0.05	3.2 (2.3–3.7)	NS

ACTH, adrenocorticotropin hormone; AUC, area under the curve; NS, not significant. Values are medians (interquartile range). Peak cortisol and cortisol AUC are the results on an ACTH stimulation test under 1-mg dexamethasone suppression.

basal ACTH levels, decreased peak cortisol levels, and the cortisol AUC on the dex-ACTH test after uADX with 80% power at the 5% level of significance (Supplementary Table 2, Supplemental Digital Content 2, http://links.lww.com/HJH/A270). In addition, the results of the dex-ACTH tests showed the same tendency in all cases. Therefore, the result that adrenal reserve function mildly decreased after uADX is convincing. Meanwhile, no patients developed clinically apparent adrenal insufficiency, and the basal cortisol levels were within the normal range in all patients and were not significantly different before and after uADX ($P=0.706$). In fact, if the basal cortisol level decreased to a lower normal range (138.0 nmol/l), we could detect the change with 99% power (Supplementary Table 2, Supplemental Digital Content 2, http://links.lww.com/HJH/A270).

We evaluated adrenocortical function 2 weeks after uADX to evaluate the risk for adrenal insufficiency as early as possible once the patient had reached a stable condition after uADX. We can consider that there was little influence of surgical intervention at 2 weeks after laparoscopic adrenalectomy [31–33]. Furthermore, in this study, six of 14 patients were observed for a longer duration to verify the long-term outcomes. In the six patients, the results 1 year after uADX showed almost the same tendency as those 2 weeks after uADX. Basal plasma ACTH levels after uADX also remained significantly higher than those before uADX. Basal serum cortisol levels remained within the normal range and were not significantly different before and 1 year after uADX (Table 3). Moreover, the cortisol response to ACTH on the dex-ACTH test 1 year after uADX did not return to the preoperative level and remained significantly decreased compared with that before uADX ($P<0.05$) (Table 3, Fig. 3). Meanwhile, the percentage of eosinophils 1 year after uADX decreased to almost the same level as that before uADX, which had increased 2 weeks after uADX (Table 3).

In conclusion, our results suggest that although the basal serum cortisol level is maintained within the normal range, the adrenal reserve cortisol secretory capacity mildly decreases after uADX in patients with APA without SCS or Cushing's syndrome. Nevertheless, more than 80% of the reserve capacity was preserved after uADX, which is compatible with the fact that patients generally exhibit no problems in daily life after uADX. Because we compared the adrenal cortisol secretory capacity before and after uADX, our data are important to understand how

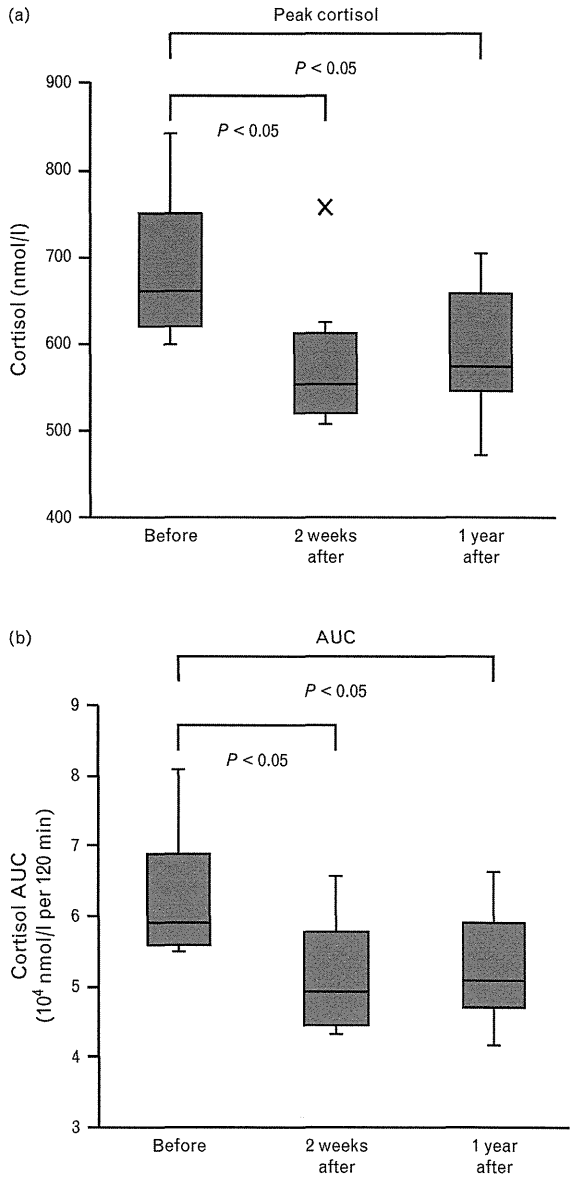

FIGURE 3 Peak cortisol levels (a) and cortisol AUC (b) on the ACTH stimulation test under 1-mg dexamethasone suppression performed before, 2 weeks after, and 1 year after unilateral adrenalectomy in six patients. ACTH, adrenocorticotropin hormone; AUC, area under the curve.